

N. A. - 1425

~~CONFIDENTIAL~~

Copy 45
RM SL50D18

Inactive

NACA

RESEARCH MEMORANDUM

for the

Bureau of Aeronautics, Department of the Navy

EFFECT OF VARIOUS MODIFICATIONS ON DRAG AND LONGITUDINAL
STABILITY AND CONTROL CHARACTERISTICS AT TRANSONIC
SPEEDS OF A MODEL OF THE XF7U-1 TAILLESS AIRPLANE

NACA WING-FLOW METHOD

TED NO. NACA DE 307

By Richard H. Sawyer and James P. Trant, Jr.

Langley Aeronautical Laboratory
Langley Air Force Base, Va.

CLASSIFIED DOCUMENT

This document contains classified information affecting the National Defense of the United States within the meaning of the Espionage Act, USC 793 and 794. The transmission or the revelation of its contents in any manner to an unauthorized person is prohibited by law. Information classified here is to be imparted only to persons on the military and naval branches of the United States, or persons of those branches and military or naval departments, the national government, its post, troops, and to United States citizens of rank 1st Lt. and above, and to United States citizens of rank 1st Lt. and above, and to United States citizens of rank 1st Lt. and above, and to United States citizens of rank 1st Lt. and above, and to United States citizens of rank 1st Lt. and above.

CLASSIFIED TO BE CANCELLED

Authority Naca R 7-2960 Date 3/11/55

By 200/FA 3/23/55

NATIONAL ADVISORY COMMITTEE FOR AERONAUTICS

WASHINGTON

APR 20 1950

~~CONFIDENTIAL~~



NATIONAL ADVISORY COMMITTEE FOR AERONAUTICS

RESEARCH MEMORANDUM

for the

Bureau of Aeronautics, Department of the Navy

EFFECT OF VARIOUS MODIFICATIONS ON DRAG AND LONGITUDINAL
STABILITY AND CONTROL CHARACTERISTICS AT TRANSONIC
SPEEDS OF A MODEL OF THE XF7U-1 TAILLESS AIRPLANE

NACA WING-FLOW METHOD

TED NO. NACA DE 307

By Richard H. Sawyer and James P. Trant, Jr.

SUMMARY

An investigation was made by the NACA wing-flow method to determine the drag, pitching-moment, lift, and angle-of-attack characteristics at transonic speeds of various configurations of a semispan model of an early configuration of the XF7U-1 tailless airplane. The results of the tests indicated that for the basic configuration with undeflected ailerator, the zero-lift drag rise occurred at a Mach number of about 0.85 and that about a five-fold increase in drag occurred through the transonic speed range. The results of the tests also indicated that the drag increment produced by -8.0° deflection of the ailerator increased with increase in normal-force coefficient and was smaller at speeds above than at speeds below the drag rise. The drag increment produced by 35° deflection of the speed brakes varied from 0.040 to 0.074 depending on the normal-force coefficient and Mach number. These values correspond to drag coefficients of about 0.40 and 0.75 based on speed-brake frontal area. Removal of the fin produced a small positive drag increment at a given normal-force coefficient at speeds during the drag rise. A large forward shift of the neutral-point location occurred at Mach numbers above about 0.90 upon removal of the fin, and also a considerable forward shift throughout the Mach number range occurred upon deflection of the speed brakes. Ailerator ineffectiveness or reversal at low deflections, similar to that determined in previous tests of the basic configuration of the model in the Mach

number range from about 0.93 to 1.0, was found for the fin-off configuration and for the model equipped with skewed (more highly sweptback) hinge-line ailerons. With the speed brakes deflected, little or no loss in the incremental pitching moment produced by deflection of the aileron from 0° to -8.0° occurred in the Mach number range from 0.85 to 1.0 in contrast to a considerable loss found in previous tests with the speed brakes off.

INTRODUCTION

As a part of the investigation of the aerodynamic characteristics of complete airplane configurations in the transonic speed range, tests have been made by the NACA wing-flow method on a 0.026-scale semispan model of an early configuration of the Chance Vought XF7U-1 airplane. The results of an investigation of the longitudinal stability and control characteristics of the basic configuration of the model have been reported in reference 1. The present paper presents the results of normal-force, pitching-moment, and angle-of-attack measurements at various aileron settings for the model with the fin removed and for the model equipped with speed brakes. Pitching-moment measurements are also presented at several aileron deflections for the model equipped with an aileron having a skewed (more highly sweptback) hinge line. Results of drag measurements are given for the basic configuration of the model with the original aileron deflected 0° and -8° , the model with the fin removed, and the model equipped with speed brakes deflected 35° . The tests covered a Mach number range from about 0.65 to 1.10.

SYMBOLS

q	effective dynamic pressure
S	wing area of model
b	twice wing span of model
\bar{c}	mean aerodynamic chord of model
C_N	normal-force coefficient $\left(\frac{\text{Normal force}}{qS} \right)$
C_M	pitching-moment coefficient referred to $0.17\bar{c}$ $\left(\frac{\text{Pitching moment}}{qS\bar{c}} \right)$

C_D	drag coefficient $\left(\frac{\text{Drag}}{qS}\right)$
ΔC_D	increment in drag coefficient
α	angle of attack
δ_a	deflection of ailerator (measured in plane normal to Y-axis of model)
M	effective Mach number
$\frac{\partial C_N}{\partial \alpha}$	slope of normal-force curve per degree
$\frac{\partial C_M}{\partial C_N}$	slope of pitching-moment curve
n.p.	neutral-point location, percent $\bar{c} \left(-100 \frac{\partial C_M}{\partial C_N} + 17\right)$
R	Reynolds number based on \bar{c}

APPARATUS AND TESTS

The tests were made by the NACA wing-flow method in which the model is mounted in the high-speed flow over the wing of an F-51D airplane.

Photographs of the 0.026-scale model equipped with an end plate at the fuselage center line are given as figures 1 and 2. A detailed three-view drawing is shown in figure 3. The geometric characteristics of the model are given in table I, which also includes the dimensions of the full-scale airplane for comparison. The model was originally equipped with five interchangeable ailerators having fixed deflections of 0° , -1.6° , -4.9° , -8.0° and -13.2° measured in a plane normal to the Y-axis of the model. The hinge line of the original ailerators was swept back 24.5° . Additional ailerators having a skewed (sweptback 35°) hinge line (see fig. 3) were constructed with fixed deflections of -4.6° and -11.2° . Details of the upper- and lower-surface speed brakes are given in figure 3. The speed brakes were wedge-shaped blocks designed to simulate 35° deflection of the actual speed brakes. The model was also equipped with a fillet, shaped to the wing contour, which filled the gap left in the wing on removal of the fin. The model was mounted on a shank which

passed through a slot in the airplane wing and was supported on a strain-gage balance. The model and balance were arranged to rotate as a unit; therefore, the balance measured the forces normal and parallel to the chord line of the model. A free-floating vane, shown in figure 2, was used to determine the direction of air flow at the model location.

The chordwise and vertical gradients of velocity over the F-51D airplane wing in the region of the model were similar to those of the tests of reference 2. The effective Mach number M and the effective dynamic pressure q were determined by integrating their distributions over the area covered by the wing of the model.

Tests of the model with the fin removed were made with the original ailerators having deflections of 0° , -4.9° , and -8.0° . The model was also tested with the fin on with the skewed-hinge-line ailerators of -4.6° and -11.2° deflection. Additional tests were made with the fin on and with the speed brakes both installed and off with the original ailerators having deflections of 0° and -8.0° . The tests were made by continuously oscillating the model through an angle-of-attack range of about -5° to 15° at about 20° per second during the high-speed flight of the F-51D airplane. Measurements were also made at fixed angles of attack of about 0° and 10° on the basic configuration with the model separated from, but in the presence of, the end plate which was fixed to the surface of the F-51D airplane wing. The gap between the fuselage and the end plate was approximately 0.007 inch. The end-plate effects determined in the tests with the model separated from, but in the presence of, the end plate were found to be negligible and hence no corrections for the end plate were applied to the results presented. Also, no measurements were made of the effects of the inlet-velocity ratio of the duct (see fig. 3) on the results presented.

Two flight-test procedures were followed in relation to the Reynolds number and Mach number ranges covered by the tests. In one procedure, three runs were made: a dive from high altitude, a dive from medium altitude, and a low-altitude, high-speed, level-flight run. Three ranges of Reynolds number were thus obtained for the range of Mach numbers covered. (See fig. 4.) In the other procedure, the tests were made by diving to a medium altitude and continuing the dive within the placard limits of the airplane to a low altitude where a pull-out and deceleration to low speed was effected. This maneuver gave the maximum Reynolds number at a given Mach number attainable within the placard limits of the airplane (fig. 4).

Typical examples of the pitching-moment, angle-of-attack, and drag data at zero normal-force coefficient as obtained in the tests at three altitudes are given in figure 5. The large amount of hysteresis evident for the angle-of-attack data was caused by unequal amounts of electrical damping in the normal-force and angle-of-attack recording circuits.

PRESENTATION OF RESULTS

The results presented are summarized in tabular form as follows:

Figure	Configuration	Results
6(a)	Basic, $\delta_a = 0^\circ$	C_D against M at $C_N = K$
6(b)	Basic, $\delta_a = -8.0^\circ$	C_D against M at $C_N = K$
6(c)	Speed brakes on, $\delta_a = 0^\circ$	C_D against M at $C_N = K$
7(a)	Fin off, $\delta_a = 0^\circ$	C_M and α against M at $C_N = K$
7(b)	Fin off, $\delta_a = -4.9^\circ$	C_M and α against M at $C_N = K$
7(c)	Fin off, $\delta_a = -8.0^\circ$	C_M and α against M at $C_N = K$
8(a)	Speed brakes on, $\delta_a = 0^\circ$	C_M and α against M at $C_N = K$
8(b)	Speed brakes on, $\delta_a = -8.0^\circ$	C_M and α against M at $C_N = K$
9	Skewed aillavators, $\delta_a = 0^\circ$, -4.6°, -11.2°	C_M against M at $C_N = K$
10(a)	Basic, $\delta_a = 0^\circ$	C_D against C_N at $M = K$
10(b)	Basic, $\delta_a = -8.0^\circ$	C_D against C_N at $M = K$
10(c)	Speed brakes on, $\delta_a = 0^\circ$	C_D against C_N at $M = K$
11(a)	Basic, $\delta_a = -8.0^\circ$ minus basic, $\delta_a = 0^\circ$	ΔC_D against M at $C_N = K$
11(b)	Speed brakes on, $\delta_a = 0^\circ$ minus basic, $\delta_a = 0^\circ$	ΔC_D against M at $C_N = K$
11(c)	Fin off, $\delta_a = 0^\circ$ minus basic, $\delta_a = 0^\circ$	ΔC_D against M at $C_N = K$
12	Fin off, $\delta_a = 0^\circ, -4.9^\circ,$ -8.0°	C_N against α at $M = K$
13	Speed brakes on, $\delta_a = 0^\circ,$ -8.0°	C_N against α at $M = K$
14	Fin off, $\delta_a = 0^\circ, -4.9^\circ,$ -8.0°	$\partial C_N / \partial \alpha$ against M
15	Speed brakes on, $\delta_a = 0^\circ,$ -8.0°	$\partial C_N / \partial \alpha$ against M
16(a)	Fin off, $\delta_a = 0^\circ$	C_M against C_N at $M = K$
16(b)	Fin off, $\delta_a = -4.9^\circ$	C_M against C_N at $M = K$
16(c)	Fin off, $\delta_a = -8.0^\circ$	C_M against C_N at $M = K$
17(a)	Speed brakes on, $\delta_a = 0^\circ$	C_M against C_N at $M = K$
17(b)	Speed brakes on, $\delta_a = -8.0^\circ$	C_M against C_N at $M = K$
18	Fin off, $\delta_a = 0^\circ, -4.9^\circ,$ -8.0°	$\partial C_M / \partial C_N$ against M
19	Speed brakes on, $\delta_a = 0^\circ,$ -8.0°	$\partial C_M / \partial C_N$ against M
20	Fin off, $\delta_a = 0^\circ, -4.9^\circ,$ -8.0°	C_M against M at $C_N = K$
21	Speed brakes on, $\delta_a = 0^\circ,$ -8.0°	C_M against M at $C_N = K$
22	Skewed aillavators, $\delta_a = 0^\circ,$ -4.6°, -11.2°	C_M against M at $C_N = K$

The pitching-moment results presented in figure 9 for the model equipped with the skewed-hinge-line aillavators also include the results of the present tests of the basic configuration with undeflected aillavator since these measurements resulted in pitching moments somewhat different from those presented in reference 1 and are believed to be more suitable for comparison with the skewed-hinge-line-aillavator results. The results shown in figure 11(c) for the configuration with the fin removed were obtained from fin-on and fin-off results (not presented), whose absolute magnitude was approximately 0.01 drag coefficient higher than results previously attained; however, the incremental drag results presented are considered to be of value. The normal-force-curve slopes $\partial C_N / \partial \alpha$ given in figures 14 and 15 were taken over the linear portion of the curves presented in figures 12 and 13. The pitching-moment-curve slopes shown in figures 18 and 19 were taken as the tangent to the curves (figs. 16 and 17) at the normal-force coefficient (also shown in figs. 18 and 19) required for level flight at 30,000 feet altitude with a wing loading of 28. Comparative results taken from reference 1 are presented in figures 12 to 22.

DISCUSSION OF RESULTS

Drag Results

The results given in figure 6 indicate that, for the basic configuration with undeflected aillavator, the zero-lift drag rise began at a Mach number of about 0.85. The drag coefficient increased from a value of 0.012 at speeds below the drag rise to a maximum of about 0.071 at a Mach number of 1.075, a five-fold increase in drag. For the basic configuration with the aillavator deflected -8.0° , the zero-lift drag rise began at about the same Mach number, but the increase in drag through the transonic range was slightly less than for the undeflected-aillavator configuration. The results for the speed brakes installed showed that the drag rise occurred at about 0.1 Mach number earlier and also indicated a slightly higher drag rise through the transonic range than for the basic configuration with undeflected aillavator.

The results presented in figure 11 indicate that the incremental drag produced by -8.0° deflection of the aillavator, in general, increased with increase in normal-force coefficient at a given Mach number. In general, the values of incremental drag produced by -8.0° deflection of the aillavator were smaller at speeds above than at speeds below the drag rise. The incremental drag coefficients produced by installation of the speed brakes showed no consistent changes with changes in normal-force coefficient and Mach number but had values of from 0.040 to 0.074 depending on the values of normal-force coefficient and Mach number. These values correspond to drag coefficients of about 0.40 and 0.75 based

on speed-brake frontal area. The incremental drag between the fin-off and fin-on configurations varied from negative values at speeds below the drag rise to positive values during the drag rise, and then to negative values at supersonic speeds. The value of incremental drag varied from 0.009 to -0.009 depending on the normal-force coefficient and Mach number. The positive values of incremental drag between the fin-off and fin-on configurations at speeds during the drag rise may be the result of a favorable effect of the fin on the flow over the outer wing panel. A positive increment in drag coefficient between the fin-off and fin-on configurations was also indicated in the tests of reference 3 at Mach numbers between about 0.94 and 0.97. It should also be noted that over the Mach number region covering the drag rise, the incremental drag results presented are subject to some inaccuracy which arises from the error of measurement of Mach number, together with the steepness of the curves of drag coefficient against Mach number in this region.

Normal-Force Results

The results given in figure 14 indicate that at Mach numbers up to about 0.85, the normal-force-curve slope of the fin-off configuration is somewhat higher at low ailerator deflections than the slope of the fin-on configuration. At Mach numbers above about 0.90, the normal-force-curve slope of the fin-off configuration is appreciably lower at all ailerator deflections than the slope of the fin-on configuration. Examination of the results shown in figure 15 indicates that there are no consistent differences in the normal-force-curve slope with speed brakes on and off except in the region near $M = 1.0$ where the slope with the speed brakes on is somewhat higher.

Longitudinal-Stability Results

The results given in figure 18 indicate that removal of the fin, in general, causes a small forward shift in the neutral point location at Mach numbers up to about 0.90 for all ailerator deflections tested. At Mach numbers above about 0.90, removal of the fin causes a considerable forward movement of the neutral-point location. With the fin removed, with increase in Mach number from about 0.91 to 0.96, a large forward shift in the neutral-point location occurs for the undeflected-ailerator configuration with the result that a negative value of the static margin (c.g. at 17 percent M.A.C.) is reached at Mach numbers between about 0.94 and 0.975. It should be noted that the ailerator deflection required for trim at these speeds, however, would be a rather large negative value because of loss of ailerator effectiveness in this region and that, for ailerator deflections of -4.9° and -8.0° , the forward shift in the neutral-point location is small and the static margin always remains positive. The results of reference 4 for the undeflected-ailerator configuration

indicated, in general, only a slight forward shift in the neutral-point location on removal of the fin for Mach numbers up to 0.90. Beyond a Mach number of 0.90, a tendency toward a forward shift is evident. The addition of the speed brakes, figure 19, resulted in a considerable forward shift in the neutral-point location throughout the Mach number range. The results of the tests of reference 4 also indicated a forward shift in the neutral-point location on addition of the speed brakes but the shift was of smaller magnitude than that of the present tests. The static margin was reduced by addition of the speed brakes to a value of 2 or 3 percent mean aerodynamic chord depending on the ailerator deflection, at Mach numbers in the region of 0.80 to 0.85.

Longitudinal-Control Effectiveness Results

The results shown in figure 20 indicate that, with the fin off, ailerator ineffectiveness or reversal at low deflections occurs over approximately the same Mach number range (0.93 to 1.0) as was found for the fin-on results (reference 1). It appears, however, that with the fin off a larger reversal of ailerator effectiveness occurs than with the fin on in this Mach number range. In general, at Mach numbers both above and below the region from 0.93 to 1.0, the ailerator effectiveness with fin off over the deflection range tested was less than the effectiveness with the fin on. The results given in figure 21 indicate that for 0° to -8.0° deflection of the ailerator, with the speed brakes on, there is little or no reduction in ailerator effectiveness in the Mach number range from 0.85 to 1.0 as is evident for the configuration with speed brakes off. The results taken from reference 4 for speed brakes on and off at ailerator deflections of 0° and -4.4° also appear to indicate, in general, less reduction in ailerator effectiveness with speed brakes on than with speed brakes off at Mach numbers from about 0.85 to 0.91. In general, at Mach numbers below and above the range from 0.85 to 1.0, the ailerator effectiveness for 0° to -8.0° ailerator deflection with speed brakes on appears to be of the same magnitude as that with speed brakes off. From an inspection of figure 22, it is evident that ailerator ineffectiveness or reversal exists in the Mach number range from 0.93 to 1.0 for the skewed-hinge-line ailerator similar to that which exists for the original ailerators.

CONCLUDING REMARKS

The results of NACA wing-flow tests of drag, normal-force, pitching-moment, lift, and angle-of-attack measurements of various configurations of a semispan model of the XF7U-1 airplane throughout the Mach number range from 0.65 to 1.10 indicated the following:

The drag increment produced by -8.0° deflection of the ailerator increased with increase in normal-force coefficient and was smaller at speeds above than at speeds below the drag rise. The drag increment produced by installation of the speed brakes varied from 0.040 to 0.074, depending on the normal-force coefficient and Mach number. These values correspond to drag coefficients of about 0.40 to 0.75 based on speed-brake frontal area. Removal of the fin produced a small positive drag increment at a given normal-force coefficient at speeds during the drag rise. A large forward shift of the neutral-point location occurred at Mach numbers above about 0.90 upon removal of the fin, and also a considerable forward shift throughout the Mach number range occurred upon installation of the speed brakes. Ailerator ineffectiveness or reversal at low deflections similar to that determined in previous tests of the basic configuration of the model in the Mach number range from about 0.93 to 1.0 was found for the fin-off configuration and for the model equipped with skewed (more highly sweptback) hinge-line ailerators. With the speed brakes installed, little or no loss in the incremental pitching moment produced by deflection of the ailerator from 0° to -8.0° occurred in the Mach number range from 0.85 to 1.0 in contrast to a considerable loss found in previous tests of the basic configuration.

Langley Aeronautical Laboratory
National Advisory Committee for Aeronautics
Langley Air Force Base, Va.

Richard H. Sawyer

Richard H. Sawyer
Aeronautical Research Scientist

James P. Trant, Jr.

James P. Trant, Jr.
Aeronautical Research Scientist

Approved:

Melvin N. Gough
Melvin N. Gough

Chief of Flight Research Division

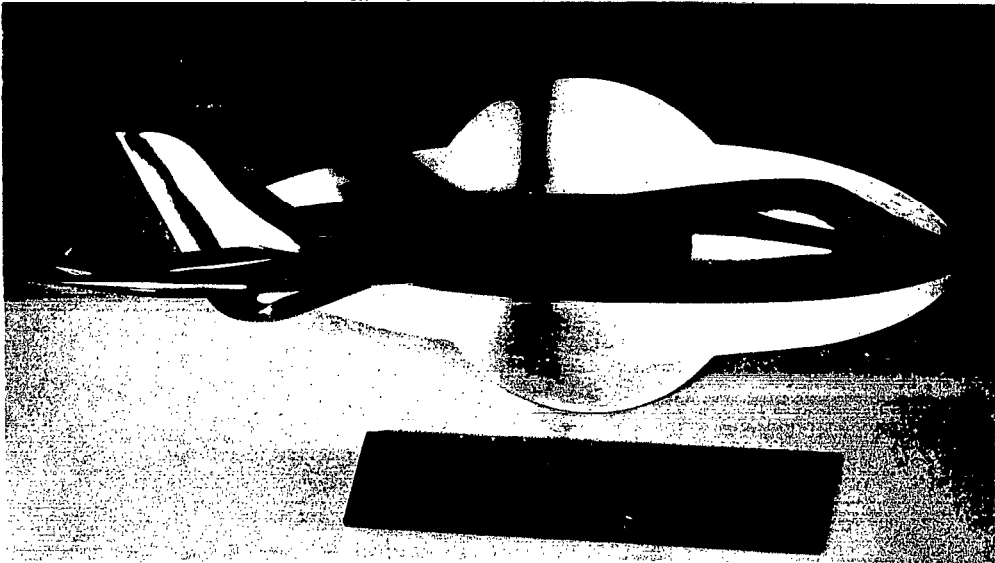
DLMcC

TABLE I

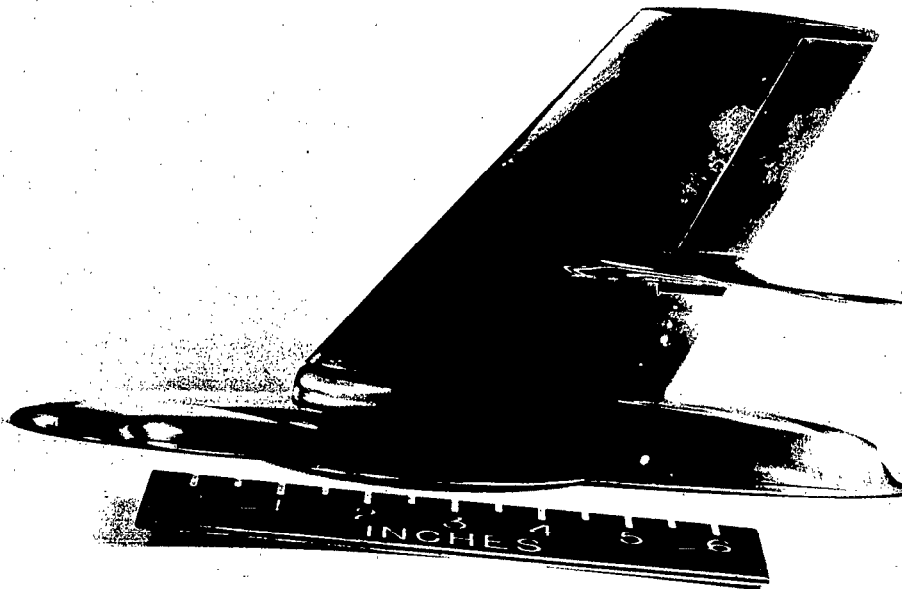
GEOMETRIC CHARACTERISTICS OF MODEL AND OF FULL-SCALE AIRPLANE

Characteristics	Model	Full-scale airplane
Wing:		
Section (perpendicular to 25-percent-chord line)	CVA4-(00)-(12)(40)-(1.1)(1.0)	CVA4-(00)-(12)(40)-(1.1)(1.0)
Semispan	6.03 in.	19 ft 4 in.
M.A.C.	4.08 in.	13 ft 1 in.
Chord at tip	3.02 in.	9 ft 8 in.
Chord at plane of symmetry	4.99 in.	16 ft 0 in.
Area (semispan)	24.2 sq in.	248 sq ft
Taper ratio	0.605	0.605
Aspect ratio	3.01	3.01
Sweepback (25-percent-chord line)	35°	35°
Incidence (constant)	0°	0°
Dihedral	0°	0°
Ailavator:		
Semispan	2.94 in.	9 ft 5 in.
Chord (parallel to plane of symmetry)	0.91 in.	35 in.
Area (one)	2.68 sq in.	27.5 sq ft
Sweepback	24.5°	24.5°
Vertical tail:		
Area of one (including wing intersection area)	6.24 sq in.	64 sq ft
Aspect ratio	1.75	1.75
Sweepback (25-percent-chord line)	40°	40°
Speed brakes:		
Area:		
Upper (one)	1.24 sq in.	12.7 sq ft
Lower (one)	1.15 sq in.	11.8 sq ft
Deflection from chord line:		
Upper	35°	35°
Lower	35°	35°
Fuselage:		
Area of maximum cross section (1/2 fuselage)	0.792 sq in.	8.14 sq ft
Area of engine bulge (one)	0.340 sq in.	3.49 sq ft
Over-all length	11.54 in.	37 ft
Air ducts:		
Area of entrance (one)	0.156 sq in.	1.60 sq ft
Area of exit (one)	0.134 sq in.	1.38 sq ft
Location of c.g.	17 percent M.A.C.	17 percent M.A.C.





NACA
L-50109



NACA
L-50106

Figure 1.- XF7U-1 semispan model. Basic configuration.

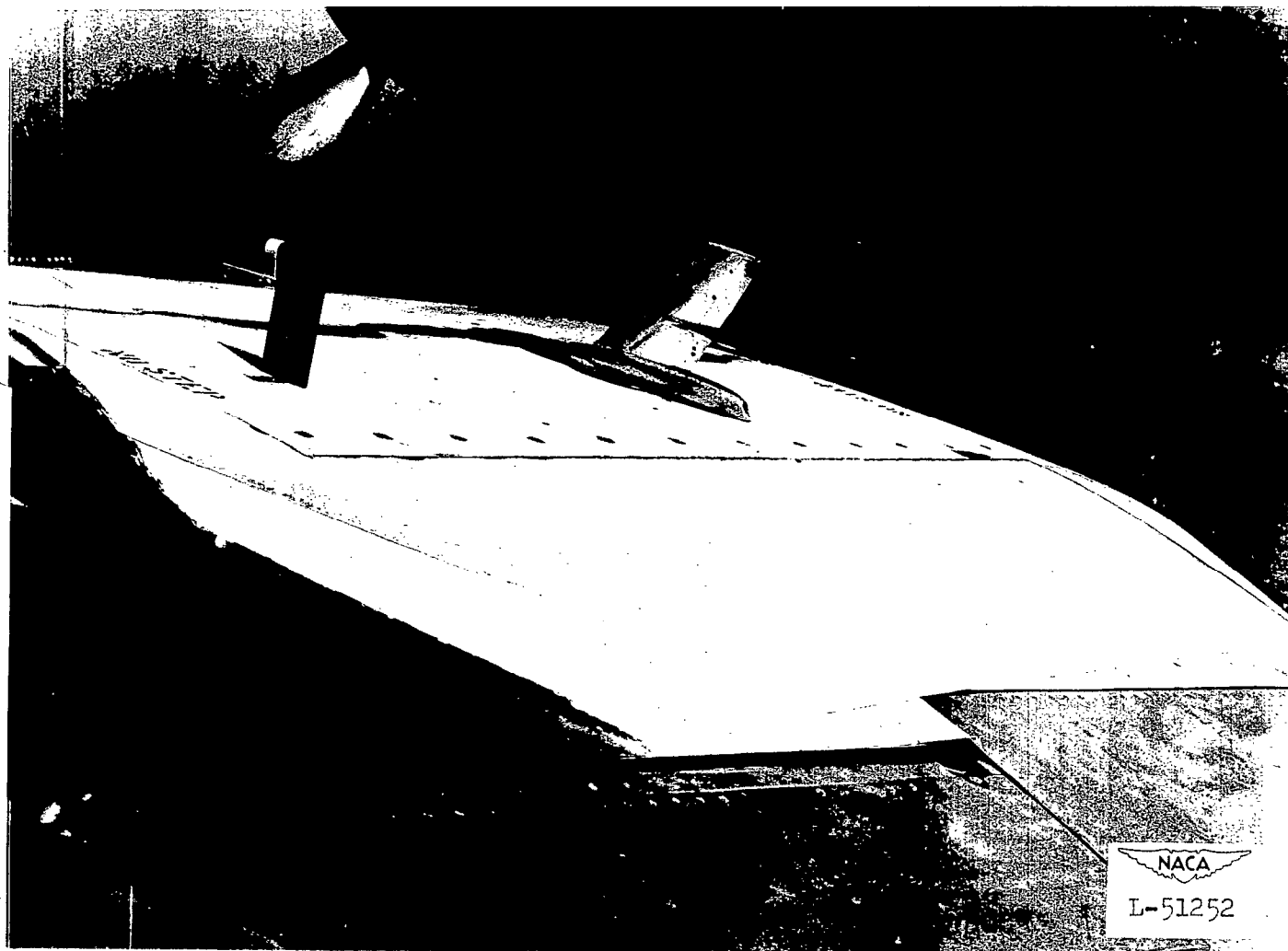
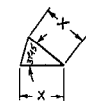
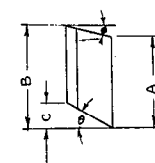
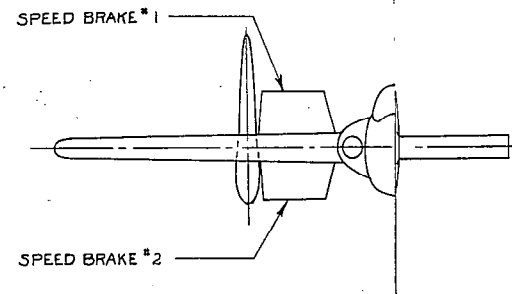
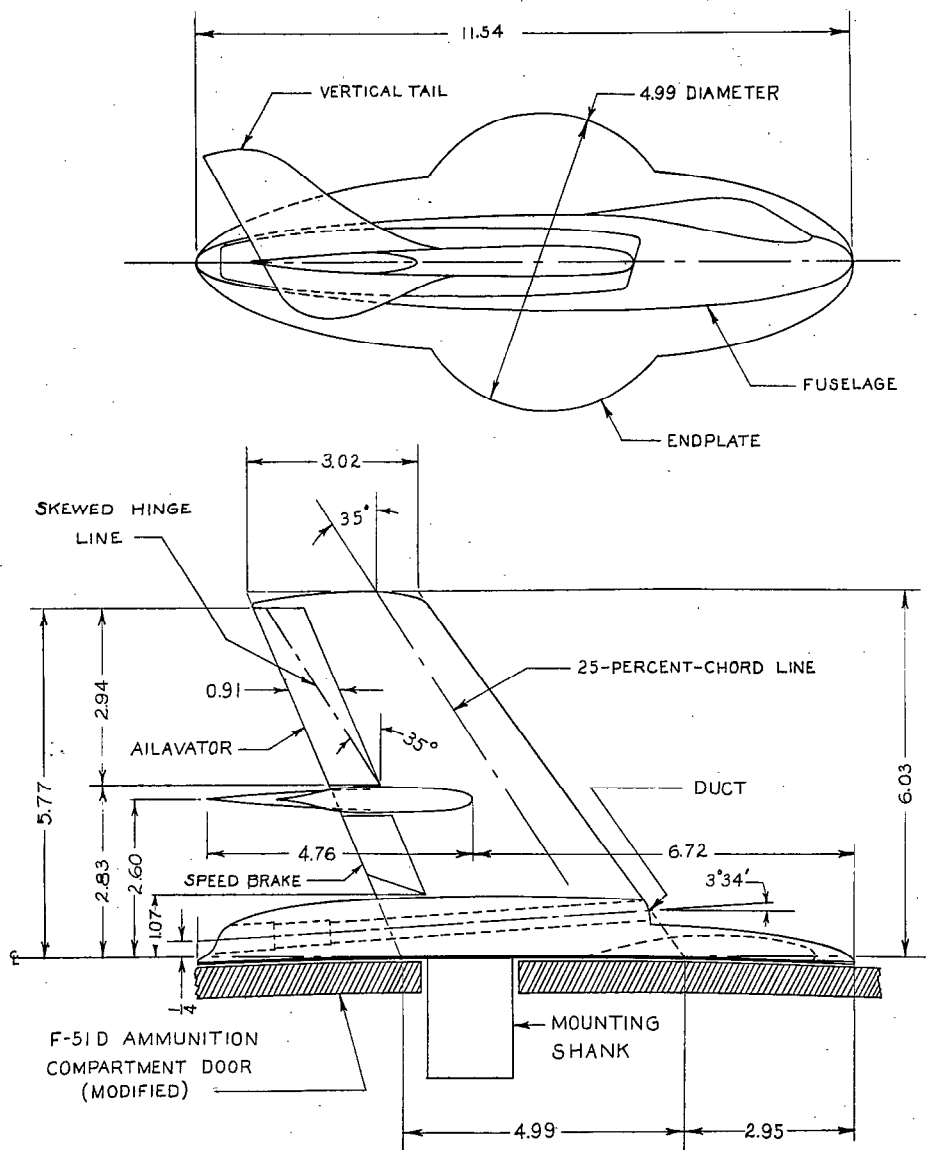


Figure 2.- XF7U-1 semispan model mounted above wing of F-51D airplane.
Free-floating vane also shown.



No.	A	B	c	e	φ	X
1	1.690	1.442	.520	29°25'	14°45'	.923
2	1.660	1.442	.470	29°25'	14°45'	.829

SPEED-BRAKE DETAILS
 #2 SHOWN */ SYM. OPP.



Figure 3.- Details of semispan XF7U-1 model. All dimensions are in inches.

~~CONFIDENTIAL~~

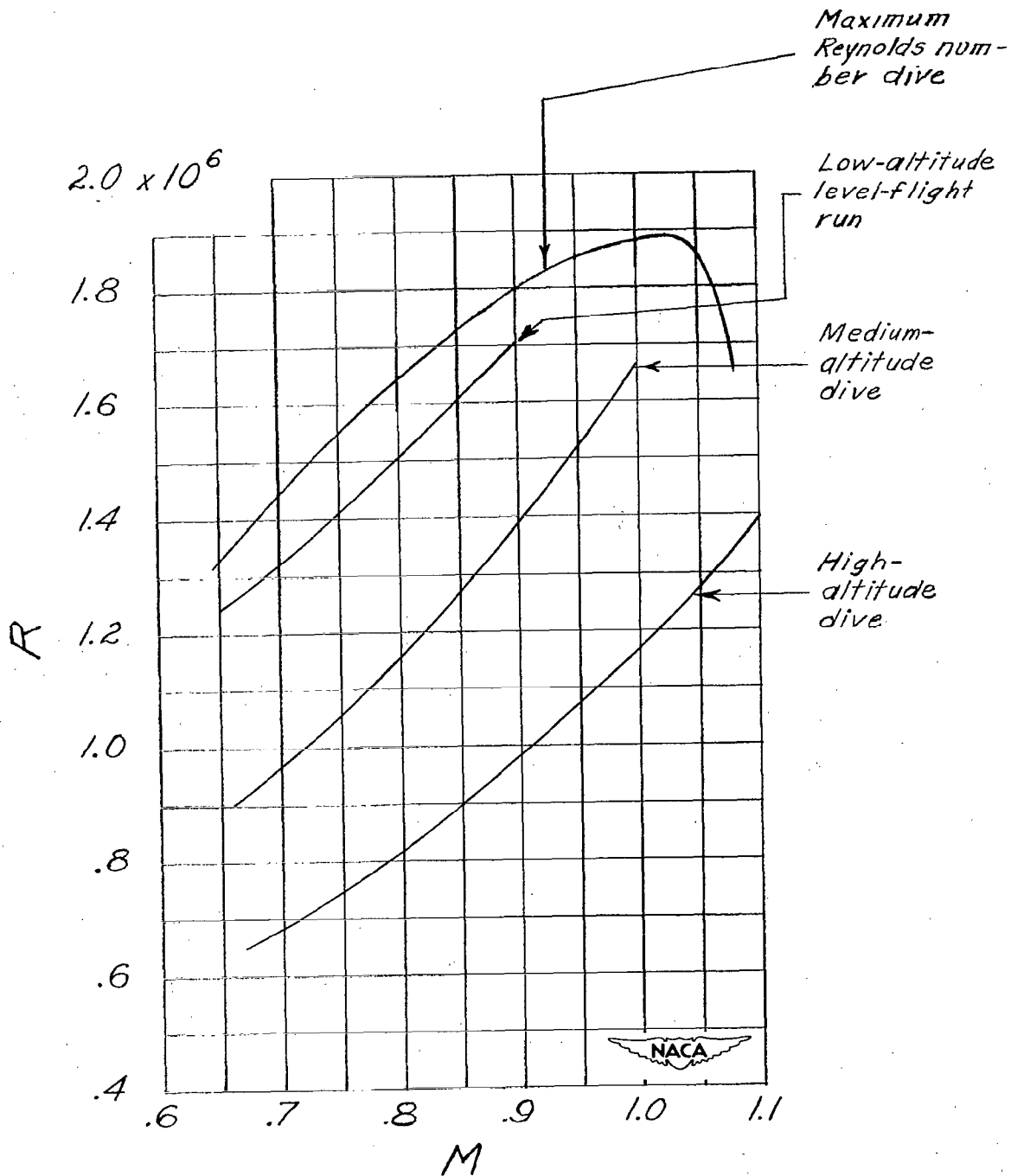


Figure 4.- Variation of Reynolds number with Mach number for tests in high-altitude and medium-altitude dives, in low-altitude, level-flight run, and in maximum Reynolds number dive.

~~CONFIDENTIAL~~

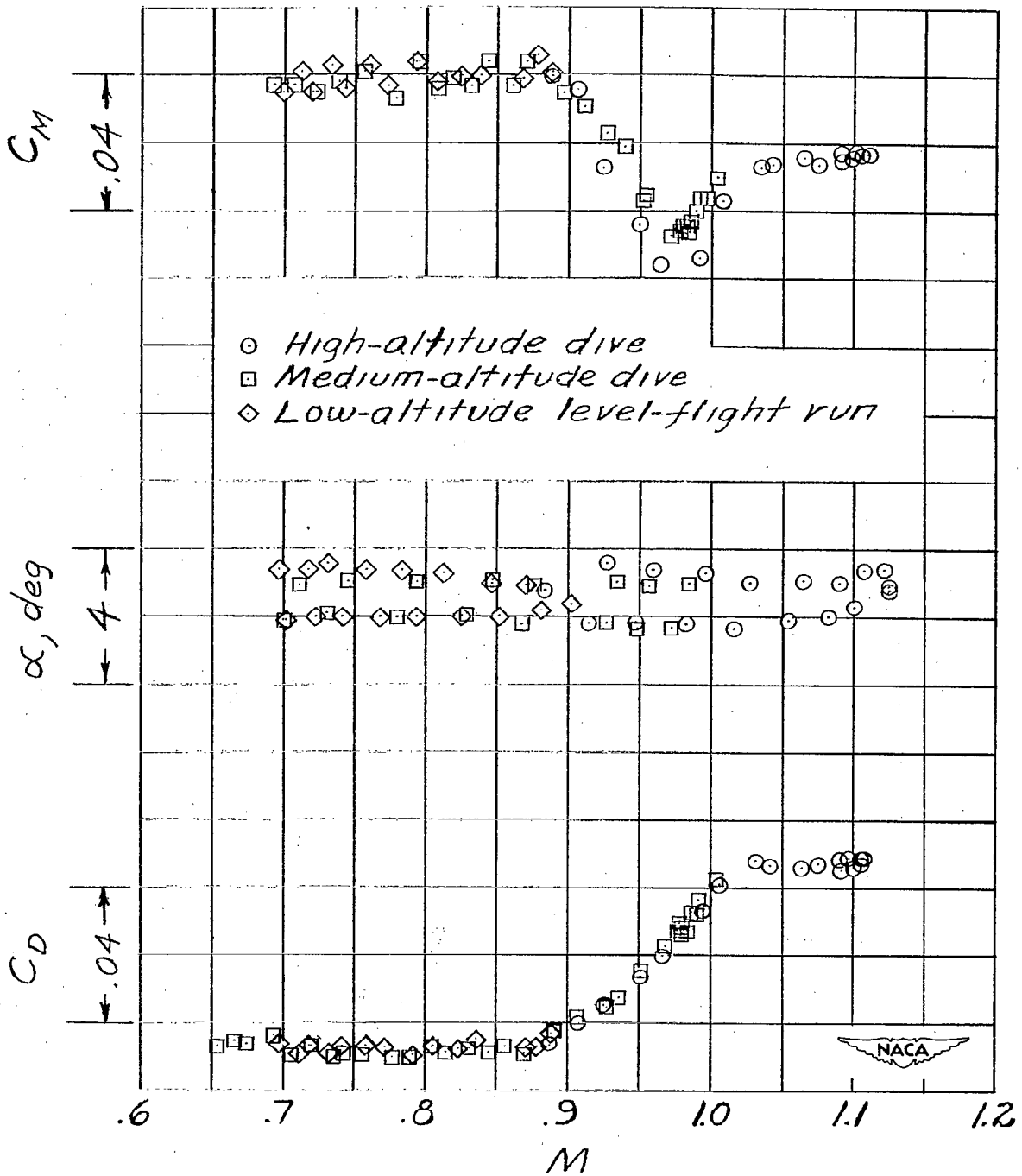
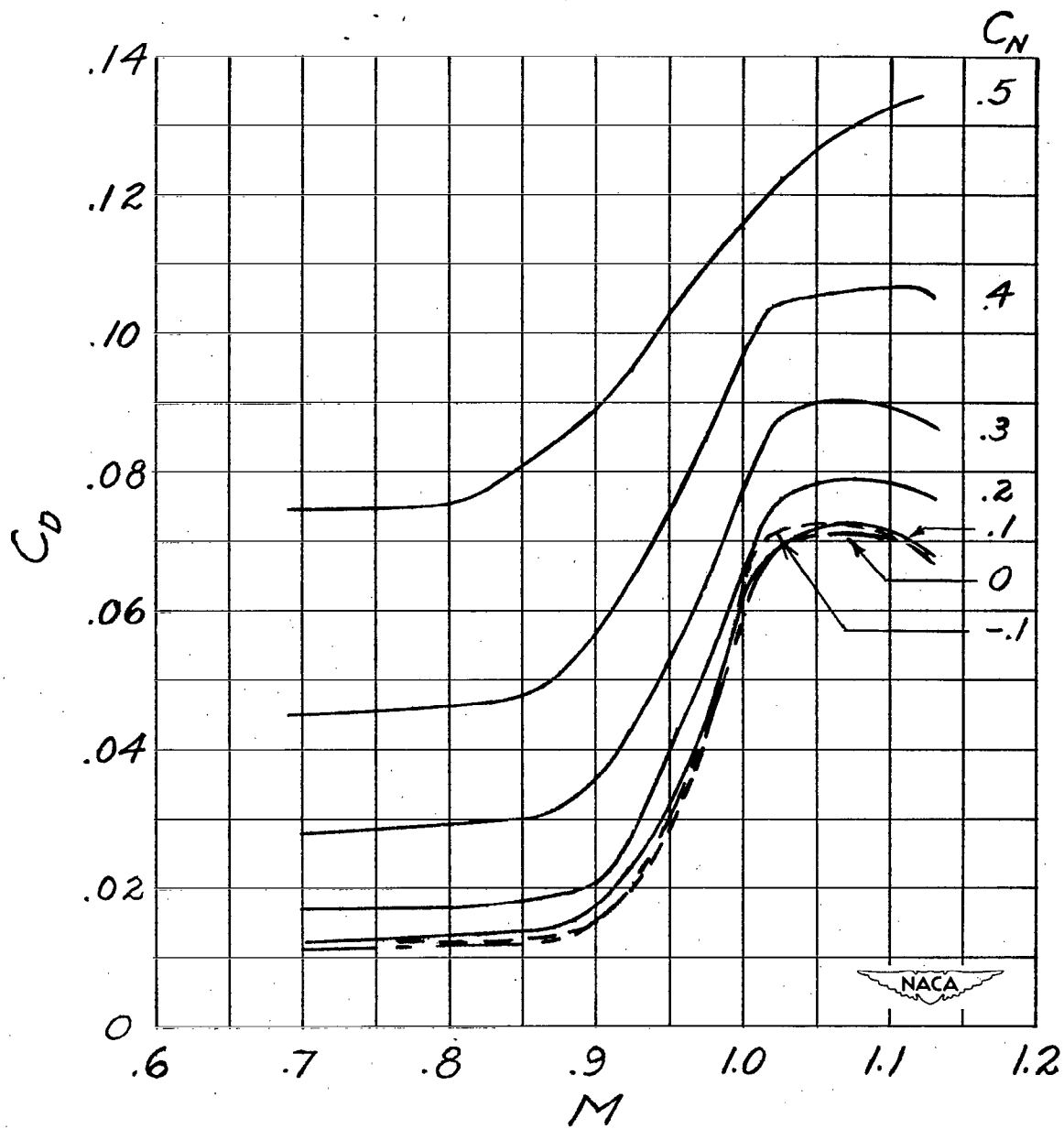
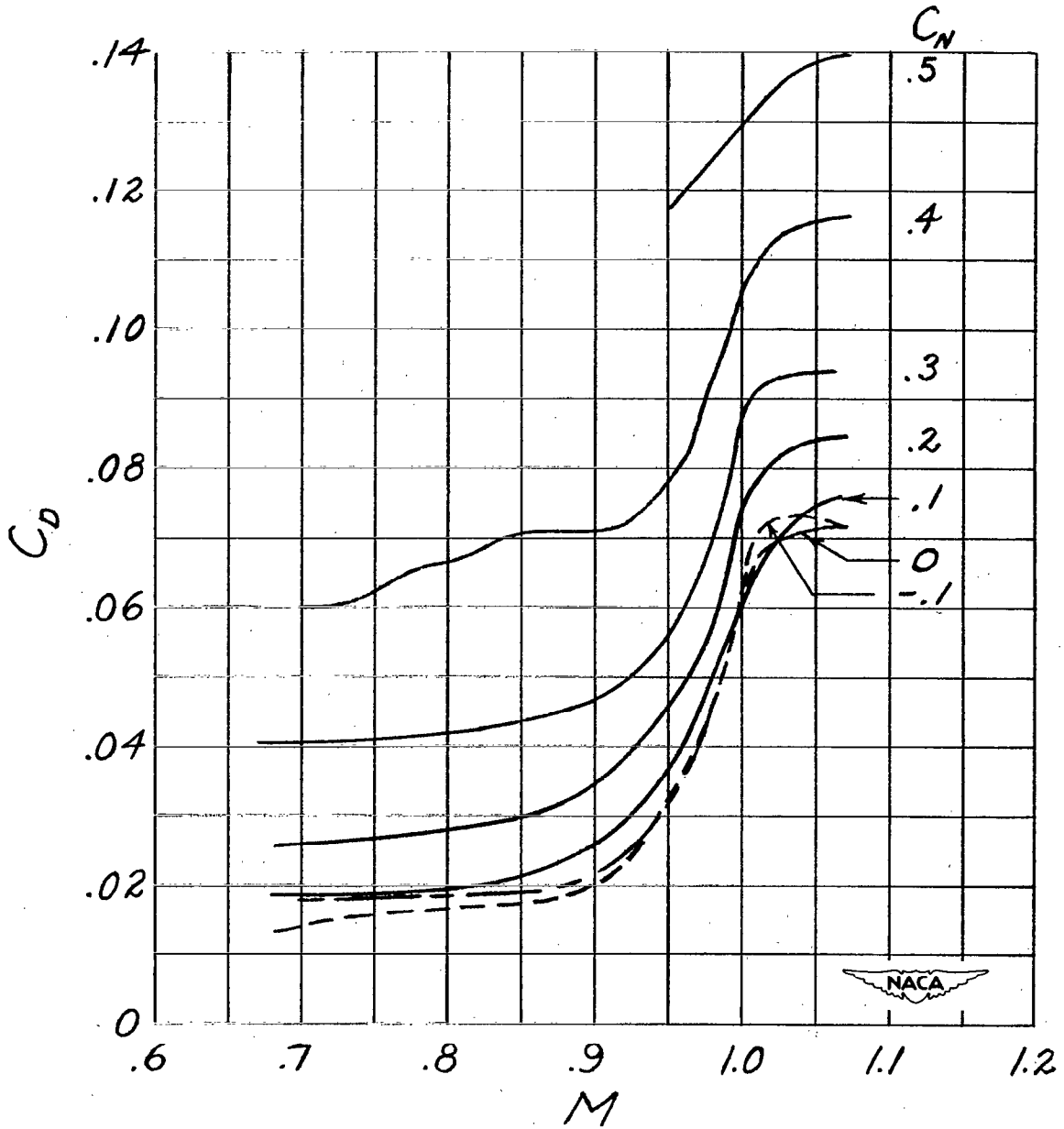


Figure 5.- Typical examples of data as obtained in tests at three altitudes. $C_N = 0$.



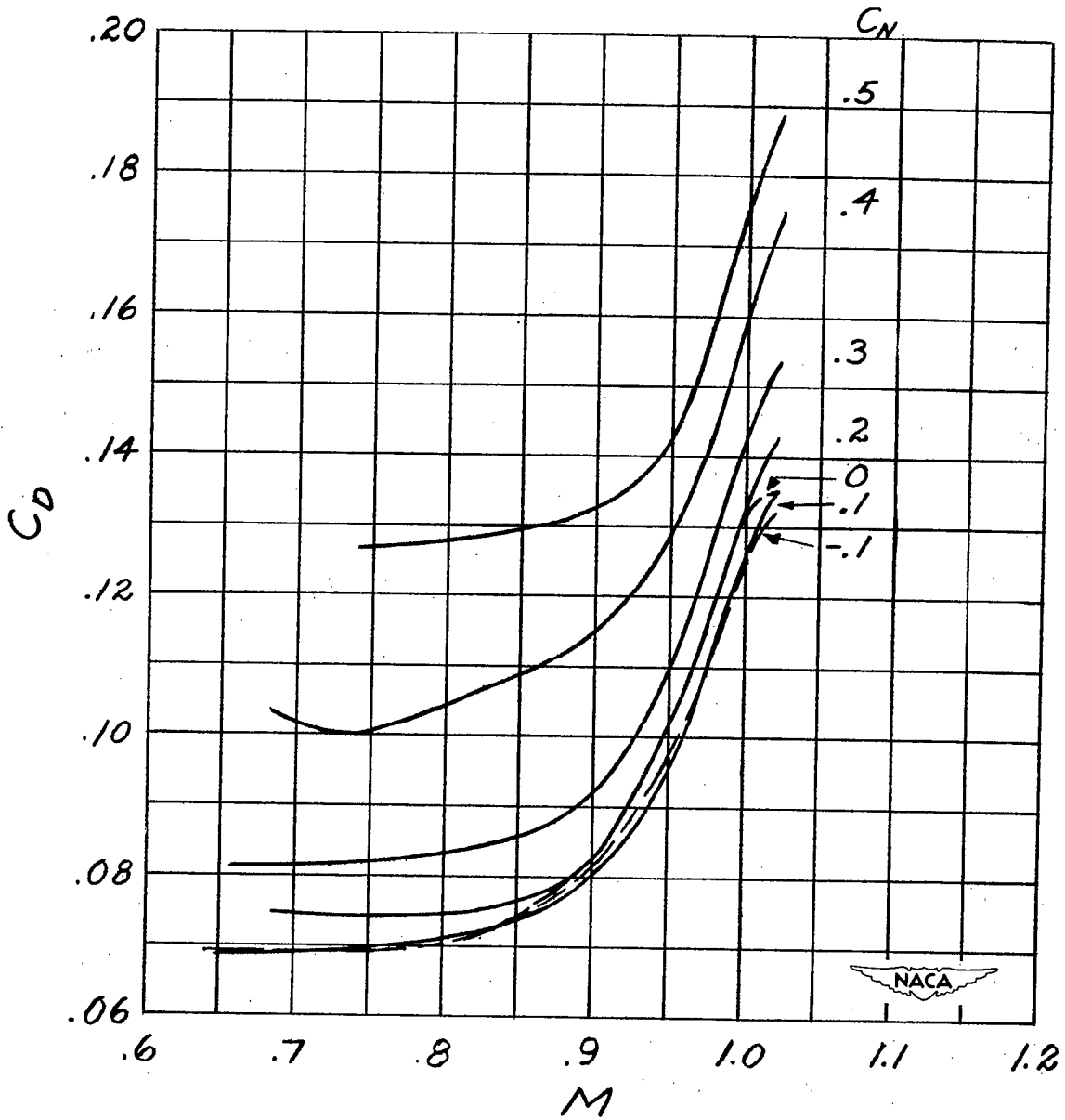
(a) Basic configuration, $\delta_a = 0^\circ$.

Figure 6.- Variation of drag coefficient with Mach number for several values of normal-force coefficient for three model configurations.



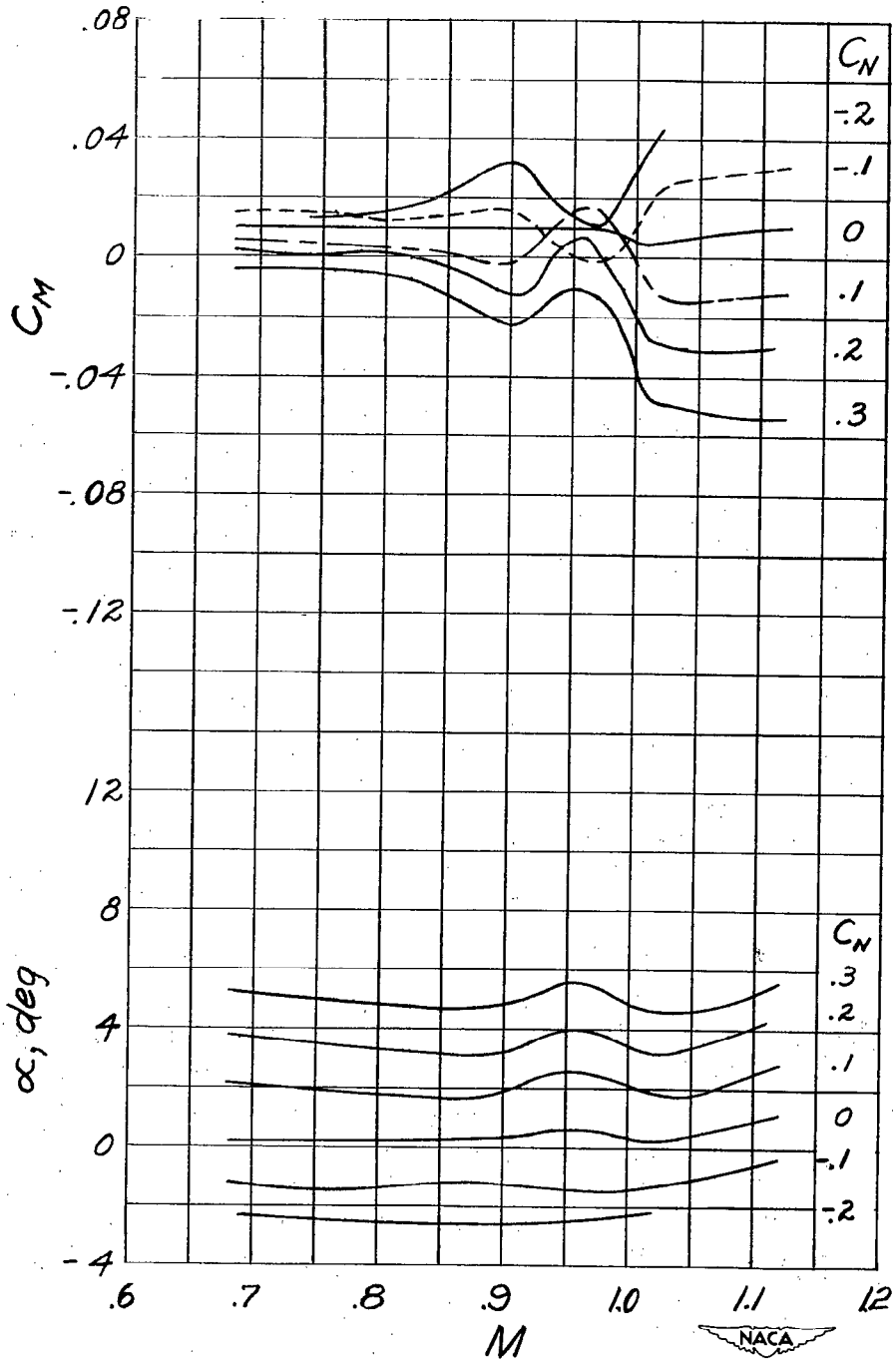
(b) Basic configuration, $\delta_a = -8^\circ$.

Figure 6.- Continued.



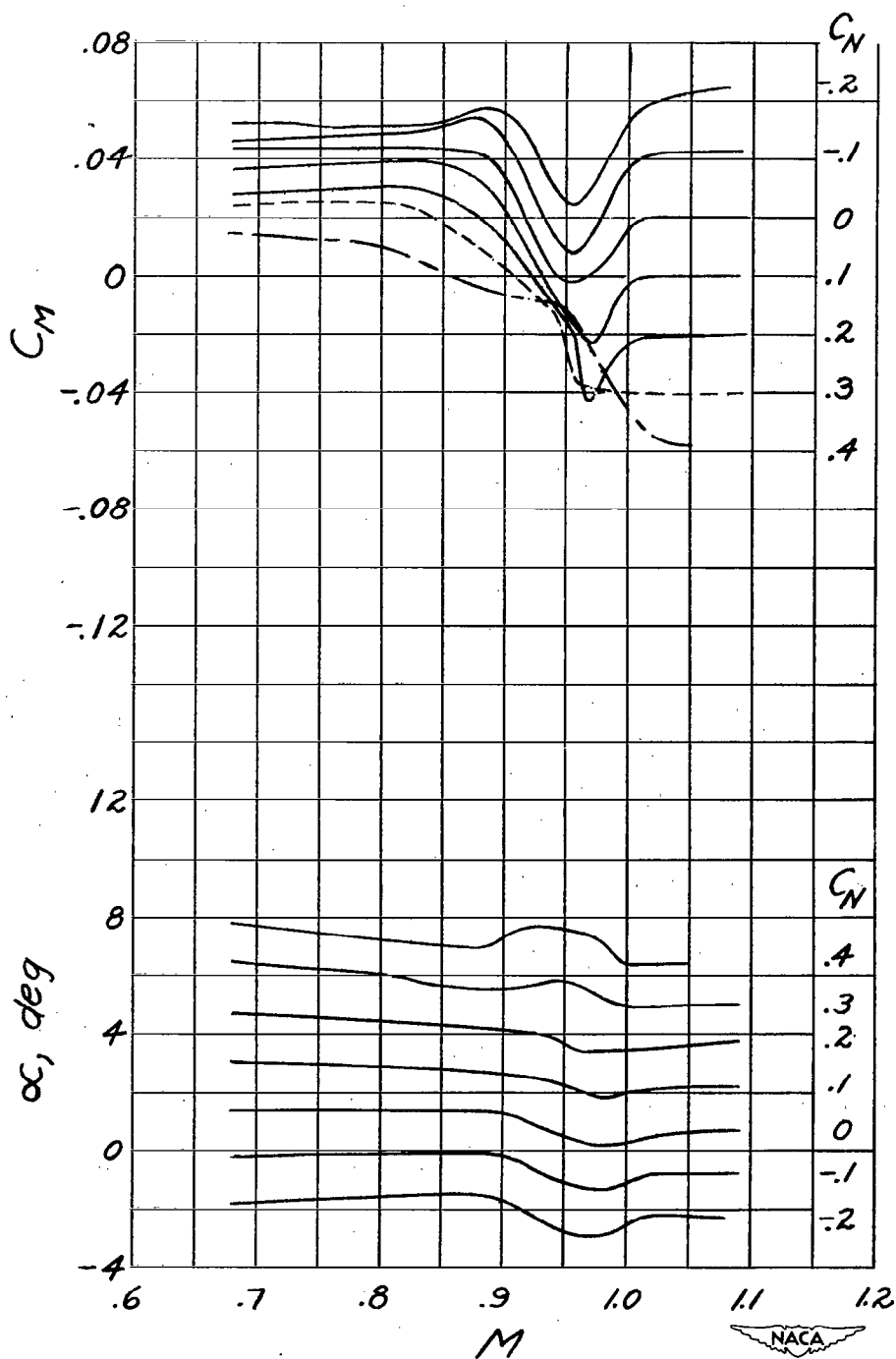
(c) Speed brakes installed. $\delta_a = 0^\circ$.

Figure 6.- Concluded.



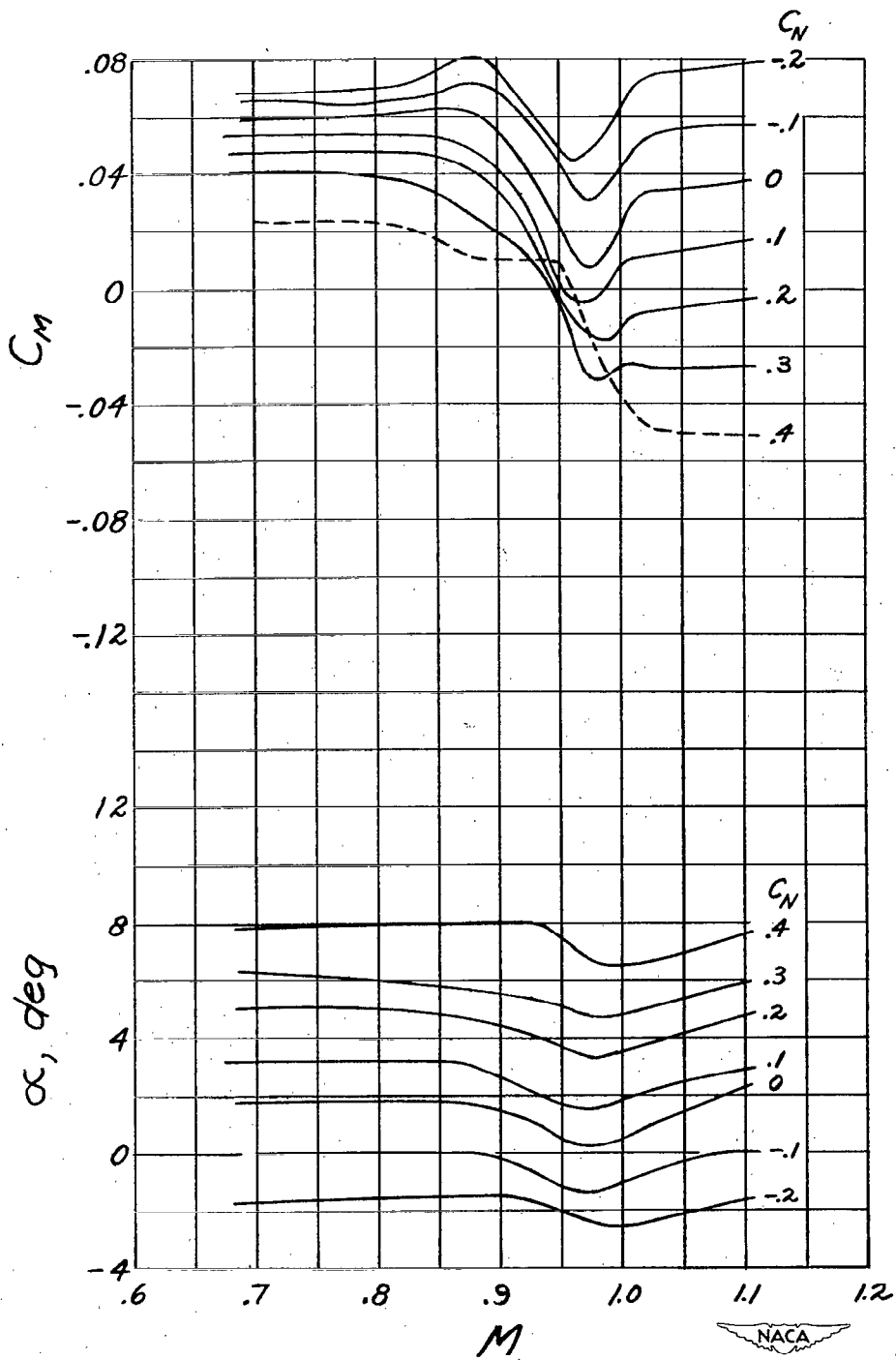
(a) $\delta_a = 0^\circ$.

Figure 7.- Variation of pitching-moment coefficient and angle of attack with Mach number at several normal-force coefficients for several allavator deflections with fin removed.



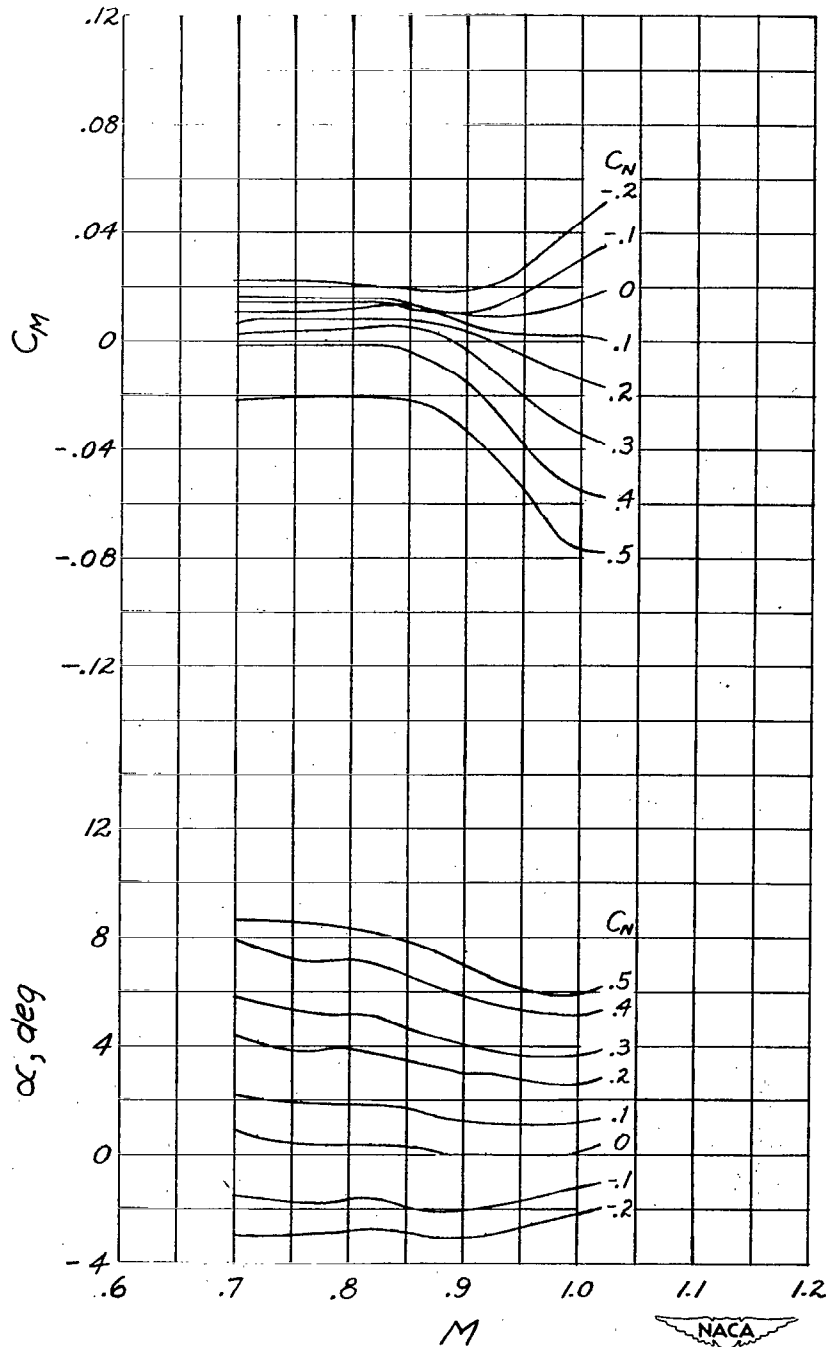
(b) $\delta_a = -4.9^\circ$.

Figure 7.- Continued.



(c) $\delta_a = -8.0^\circ$.

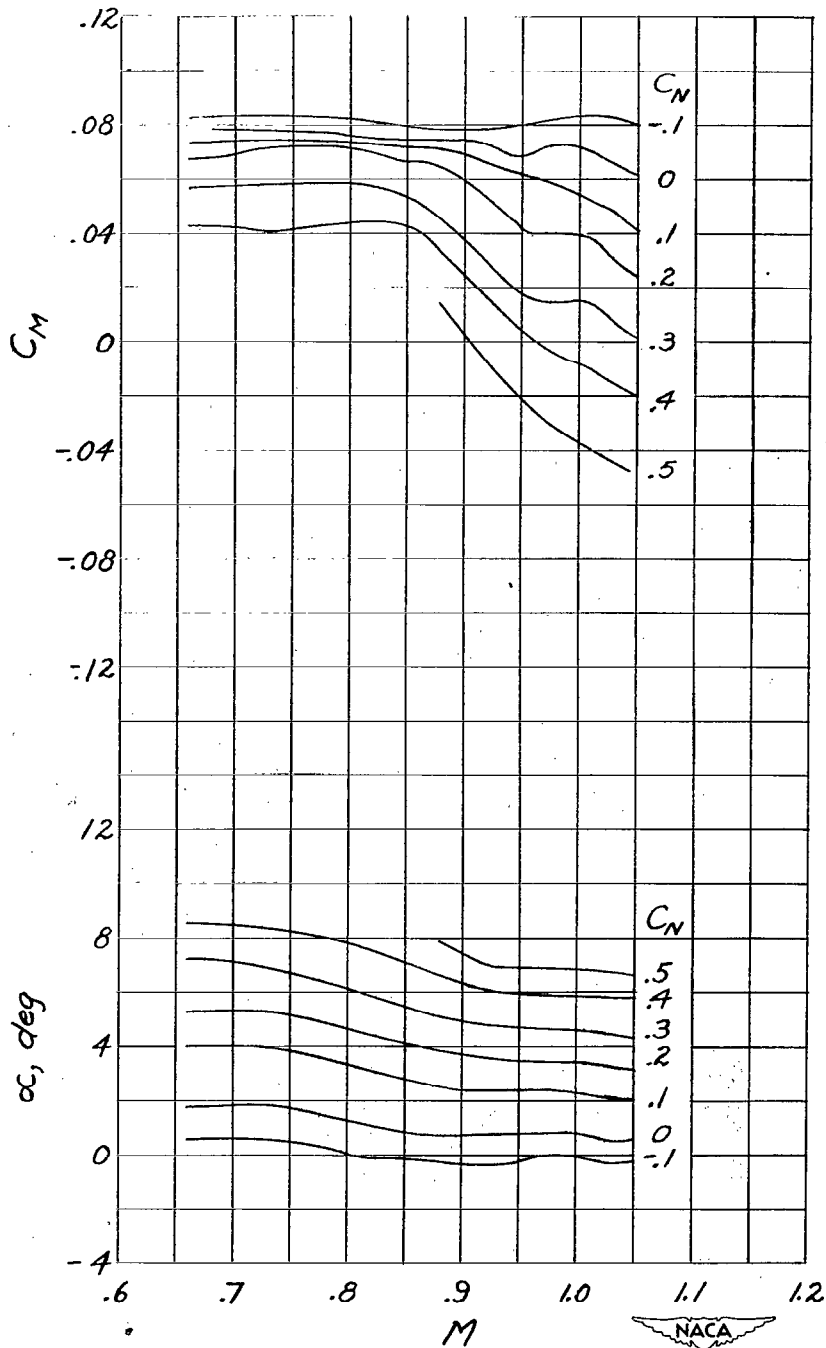
Figure 7.- Concluded.



(a) $\delta_a = 0^\circ$.

Figure 8.- Variation of pitching-moment coefficient and angle of attack with Mach number at several normal-force coefficients for two aillavator deflections with speed brakes installed.

~~CONFIDENTIAL~~



(b) $\delta_a = -8.0^\circ$.

Figure 8.- Concluded.

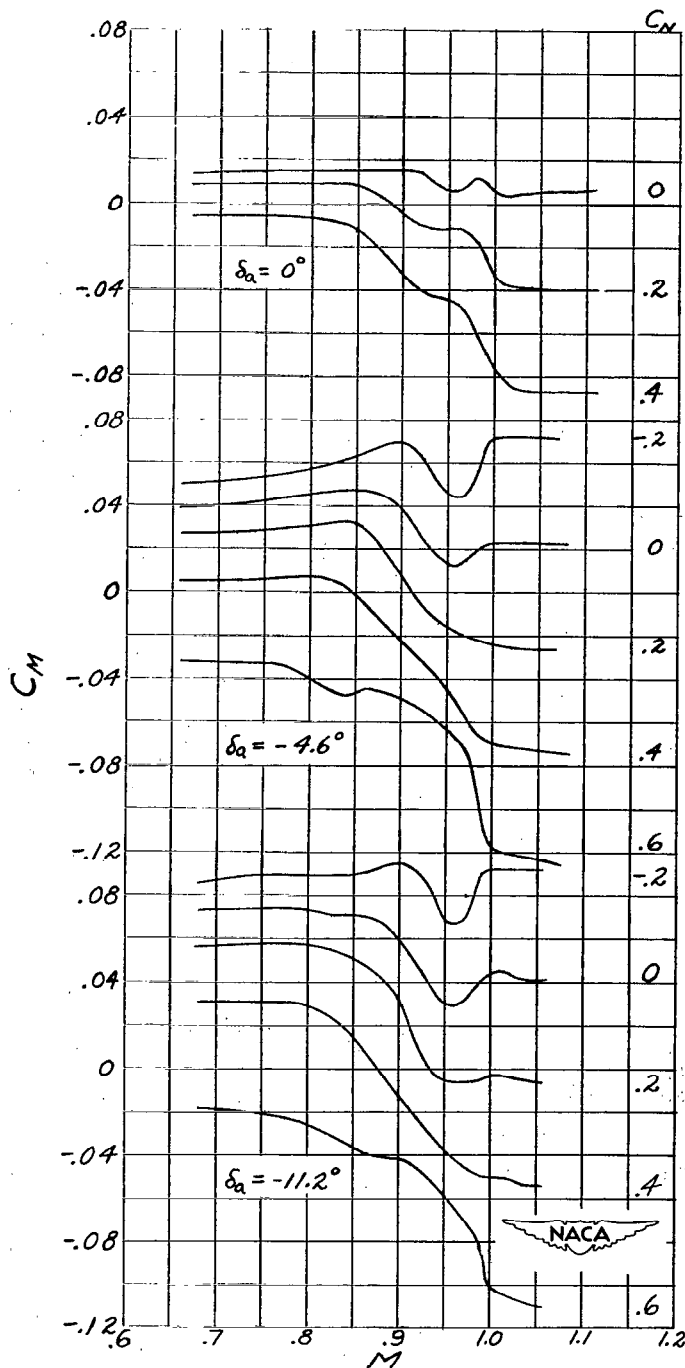
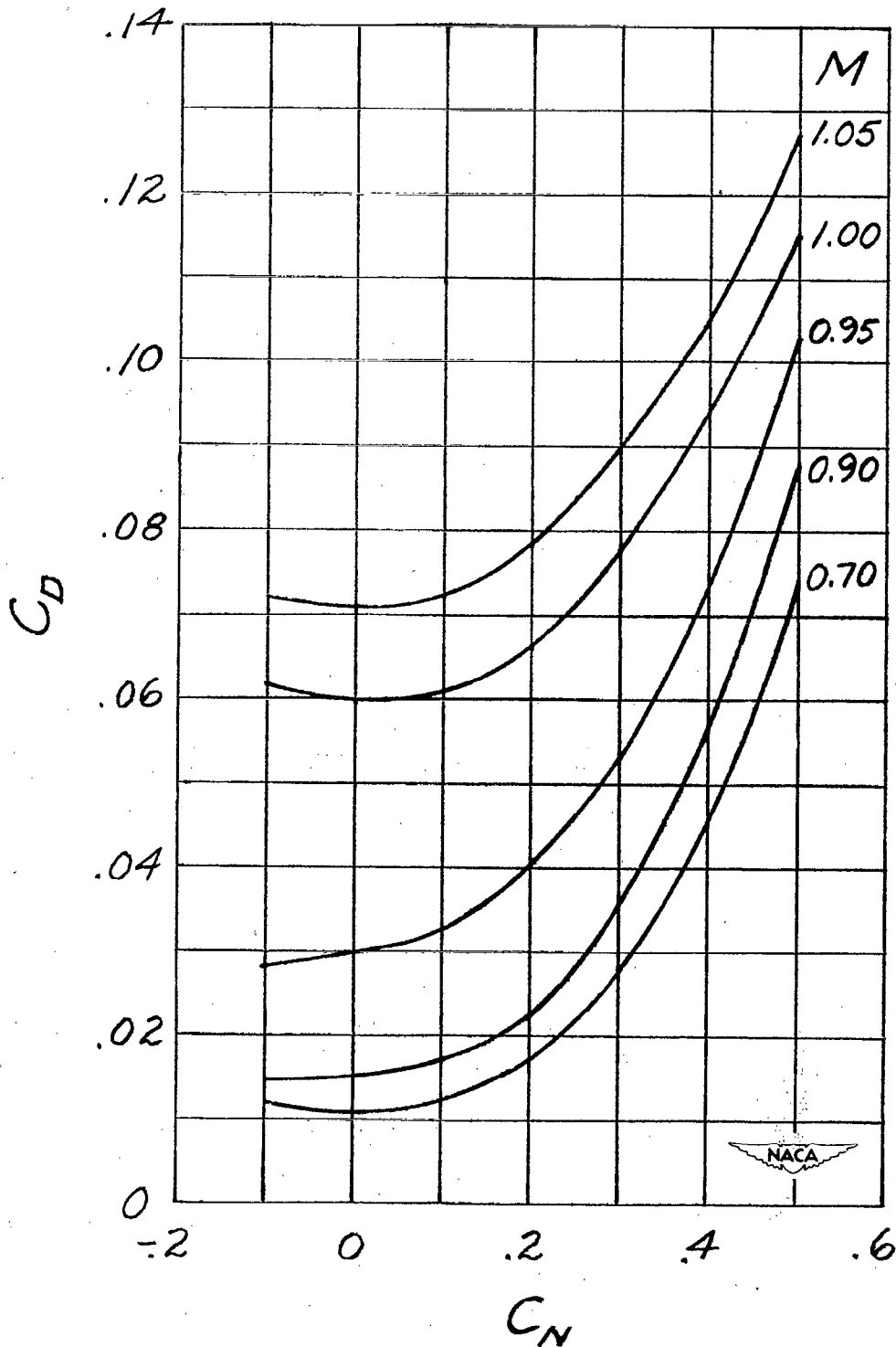
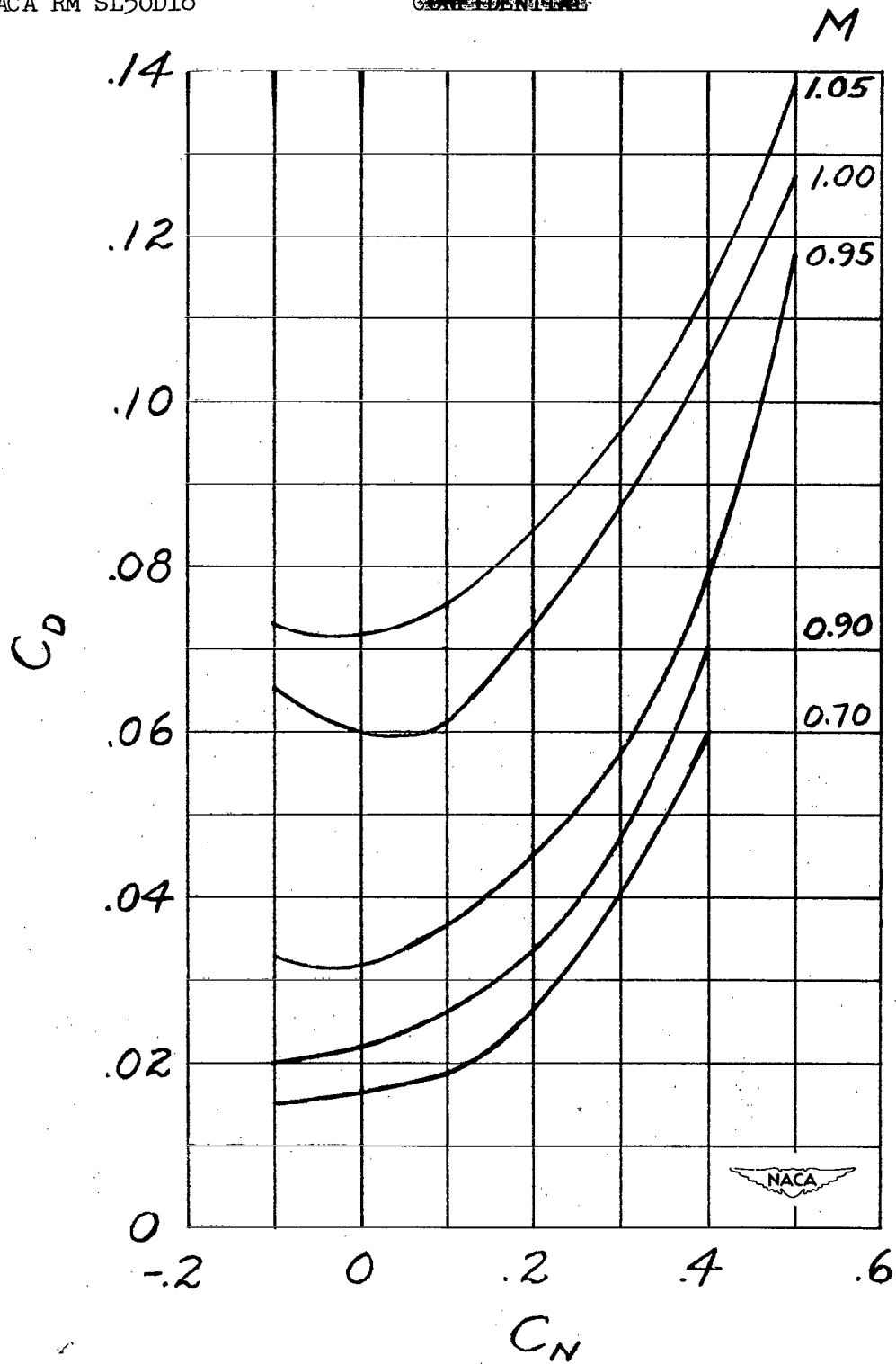


Figure 9.- Variation of pitching-moment coefficient with Mach number at several normal-force coefficients for several deflections of ailerators with highly sweptback hinge line.



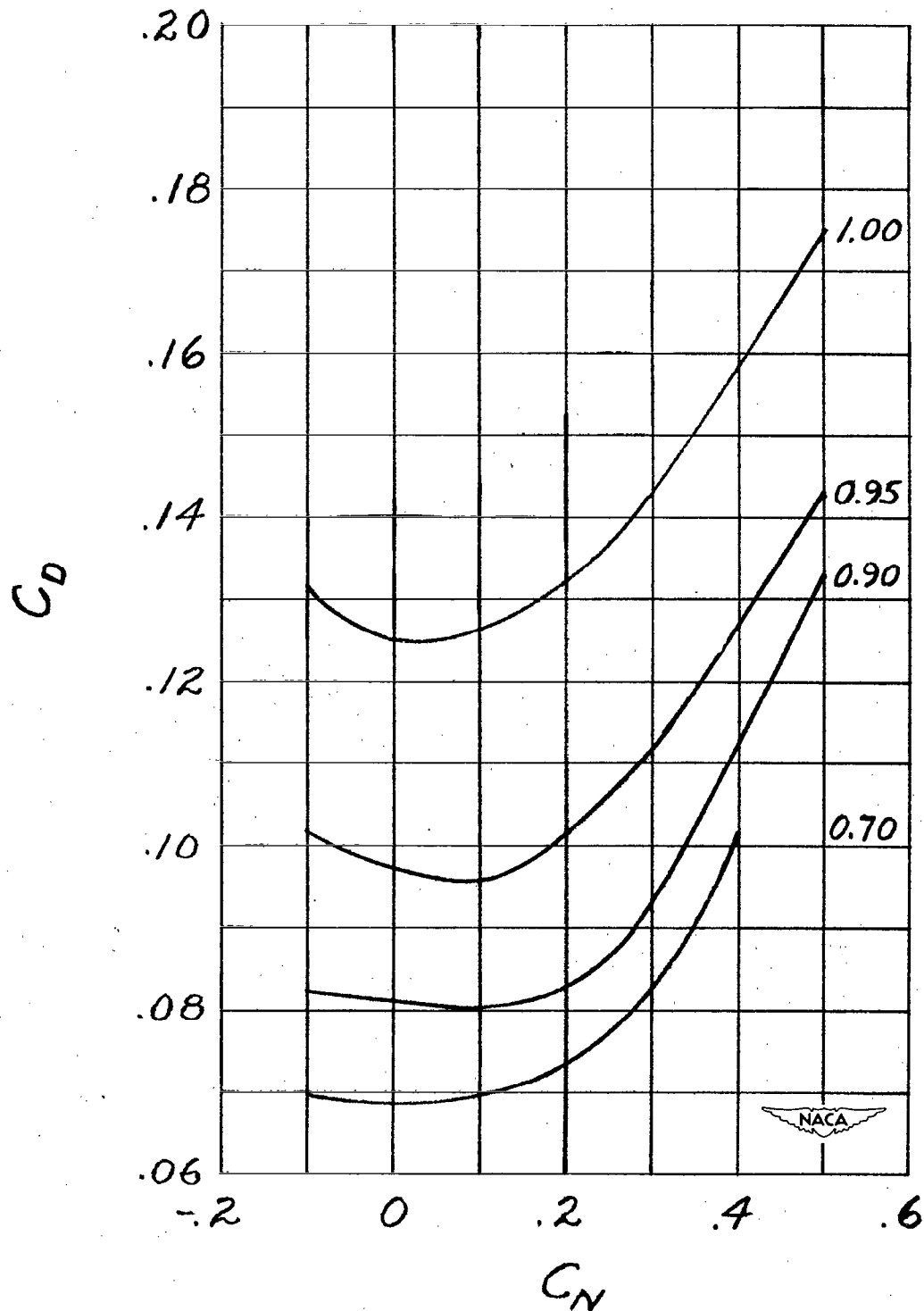
(a) Basic configuration, $\delta_a = 0^\circ$.

Figure 10.- Variation of drag coefficient with normal-force coefficient at several values of Mach number for three model configurations.



(b) Basic configuration, $\delta_a = -8^\circ$.

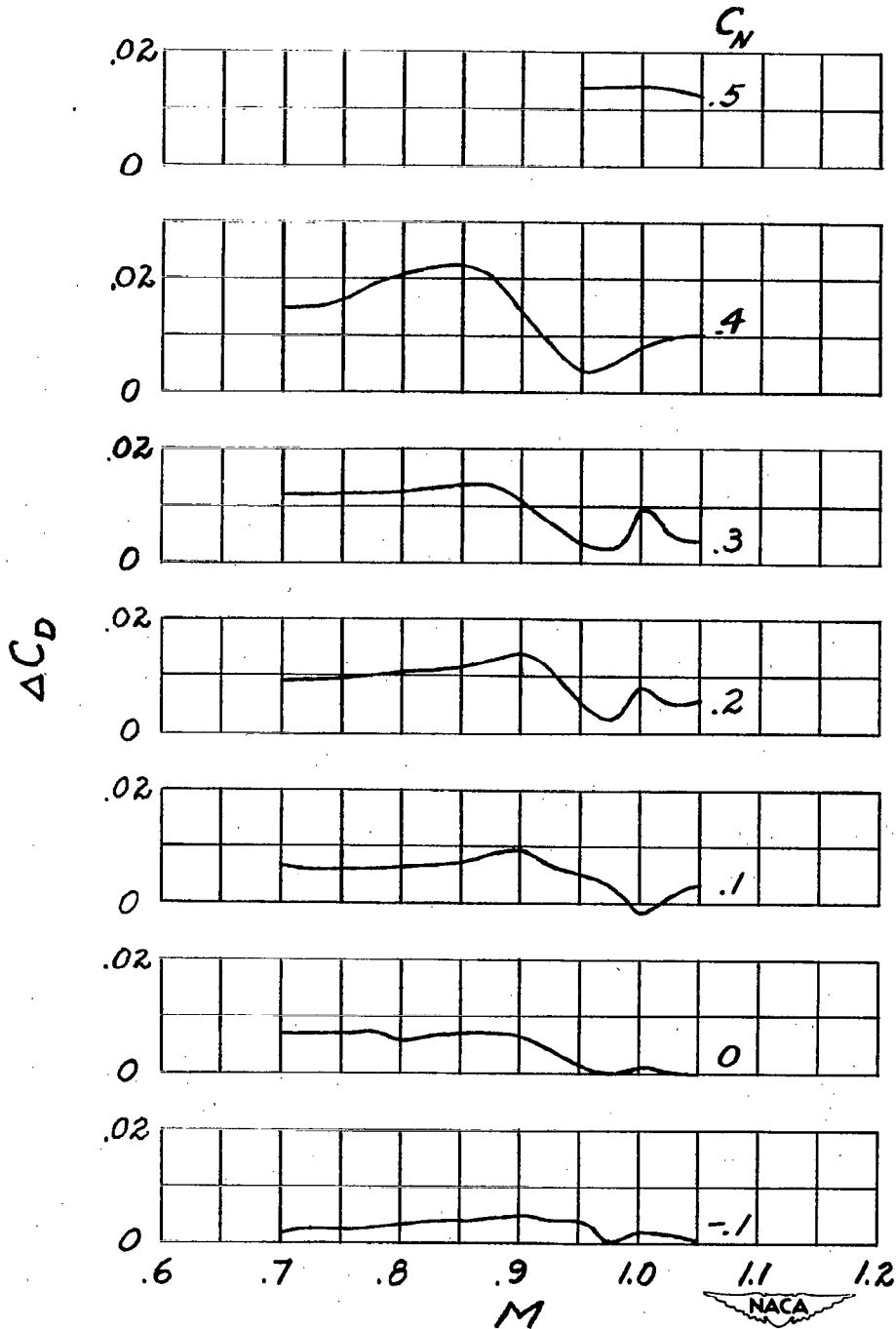
Figure 10.- Continued.



(c) Speed brakes installed, $\delta_a = 0^\circ$.

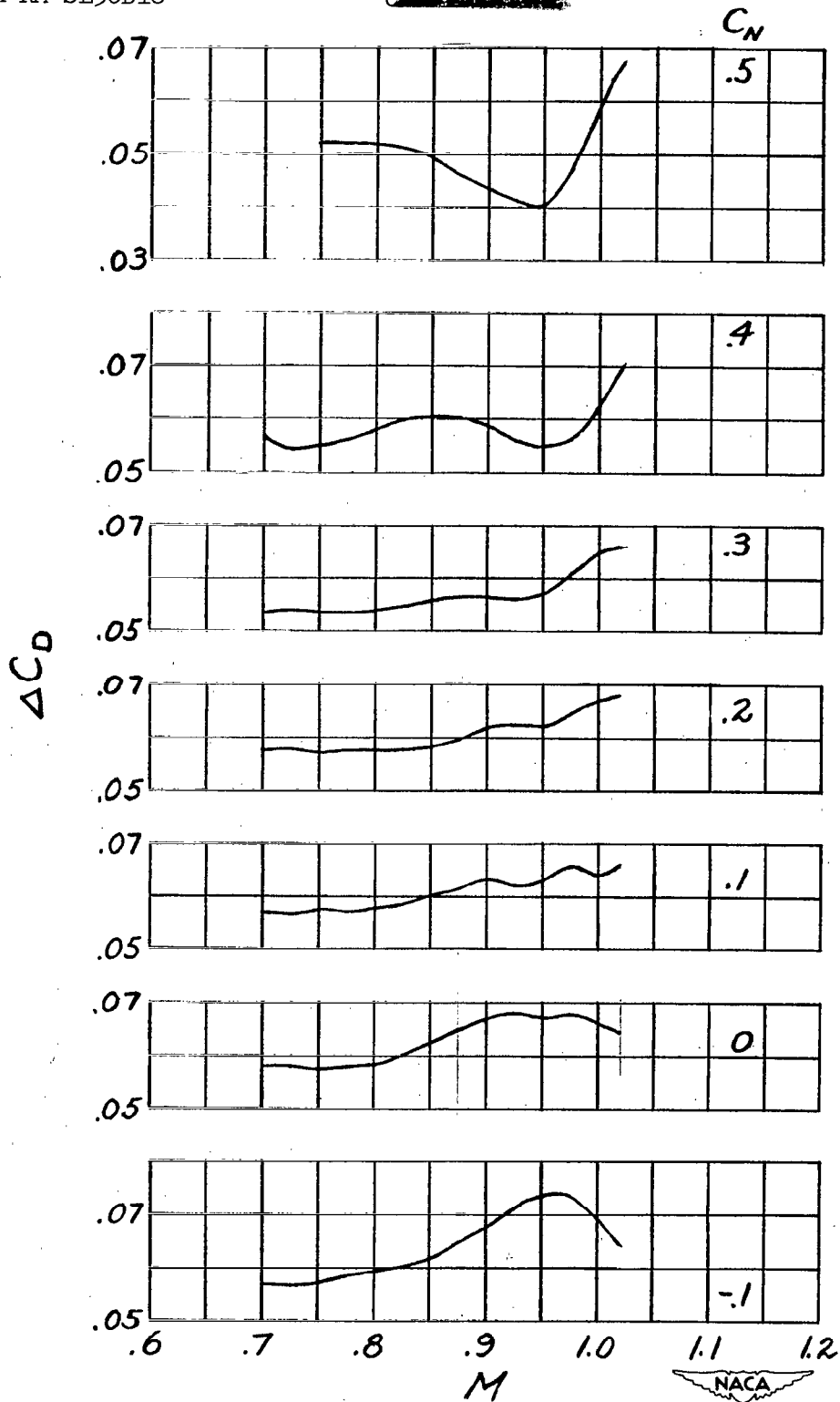
Figure 10.- Concluded.

~~CONFIDENTIAL~~



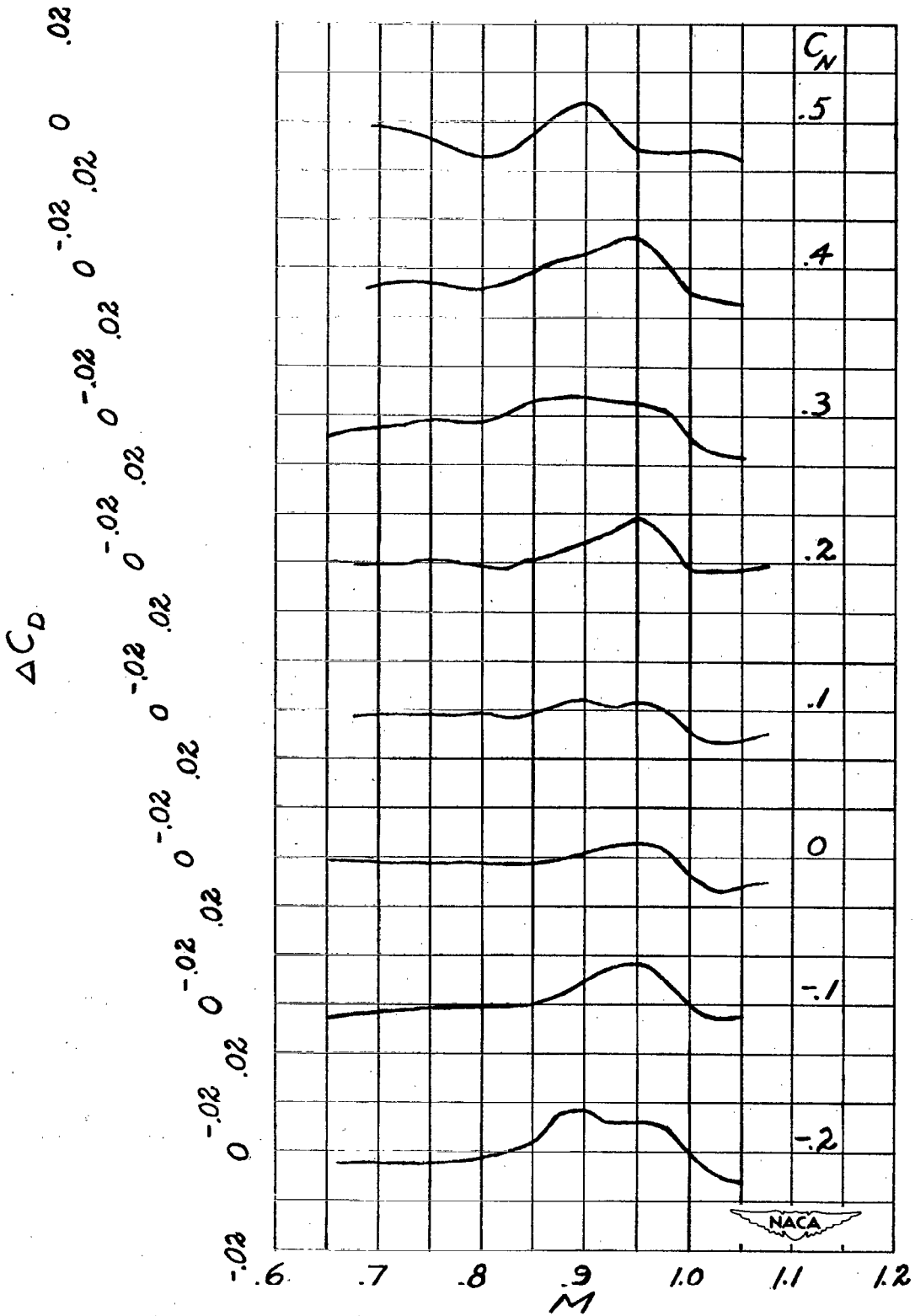
(a) Ailavator deflection of -8° .

Figure 11.- Variation of increment in drag coefficient with Mach number at several normal-force coefficients for several changes in model configuration from the basic configuration with undeflected ailavator.



(b) Installation of speed brakes.

Figure 11.- Continued.



(c) Removal of vertical tail.

Figure 11.- Concluded.

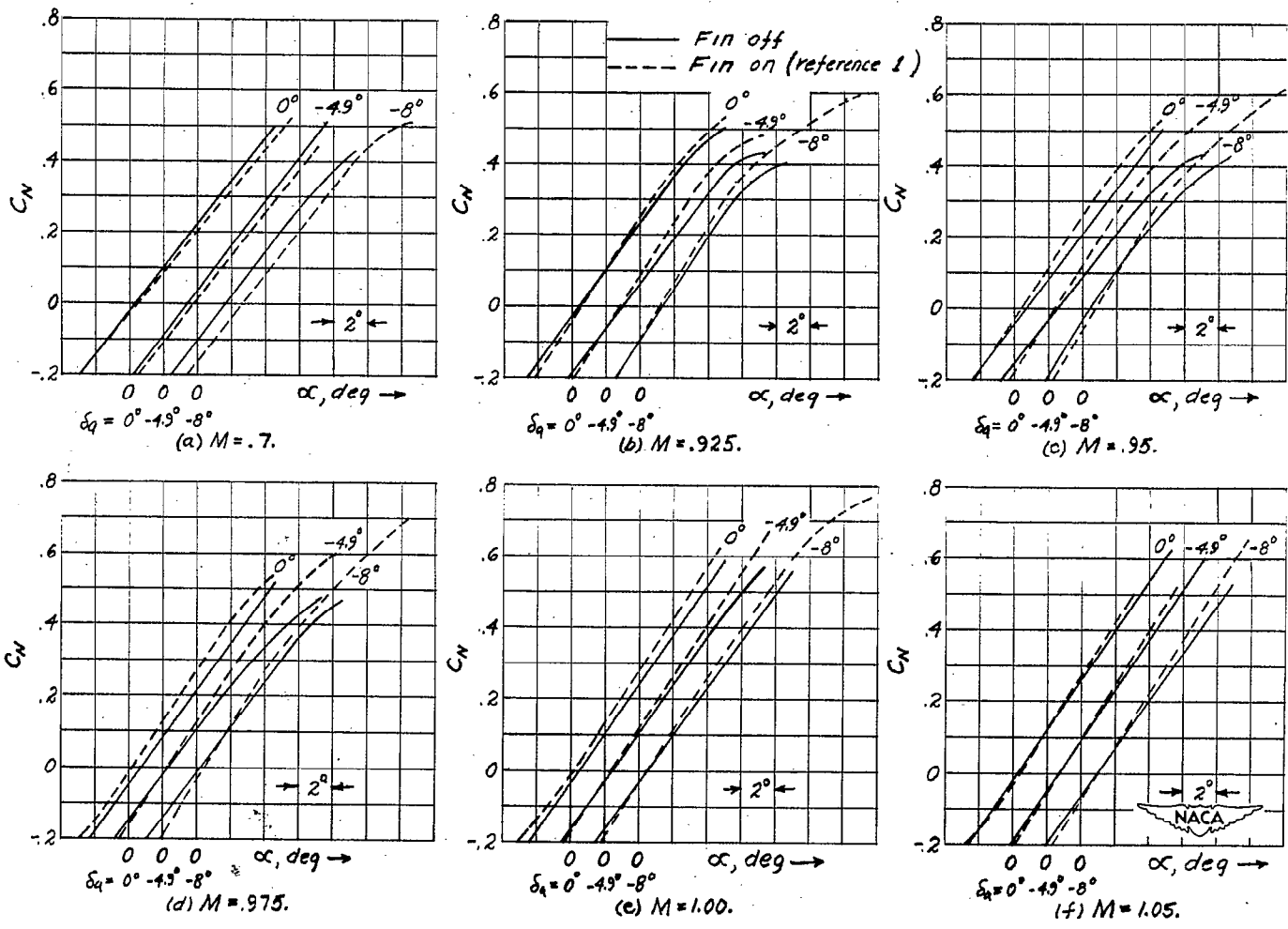


Figure 12.- Variation of normal-force coefficient with angle of attack at several Mach numbers for several ailerator deflections with fin removed. Results from reference 1 with fin on shown for comparison.

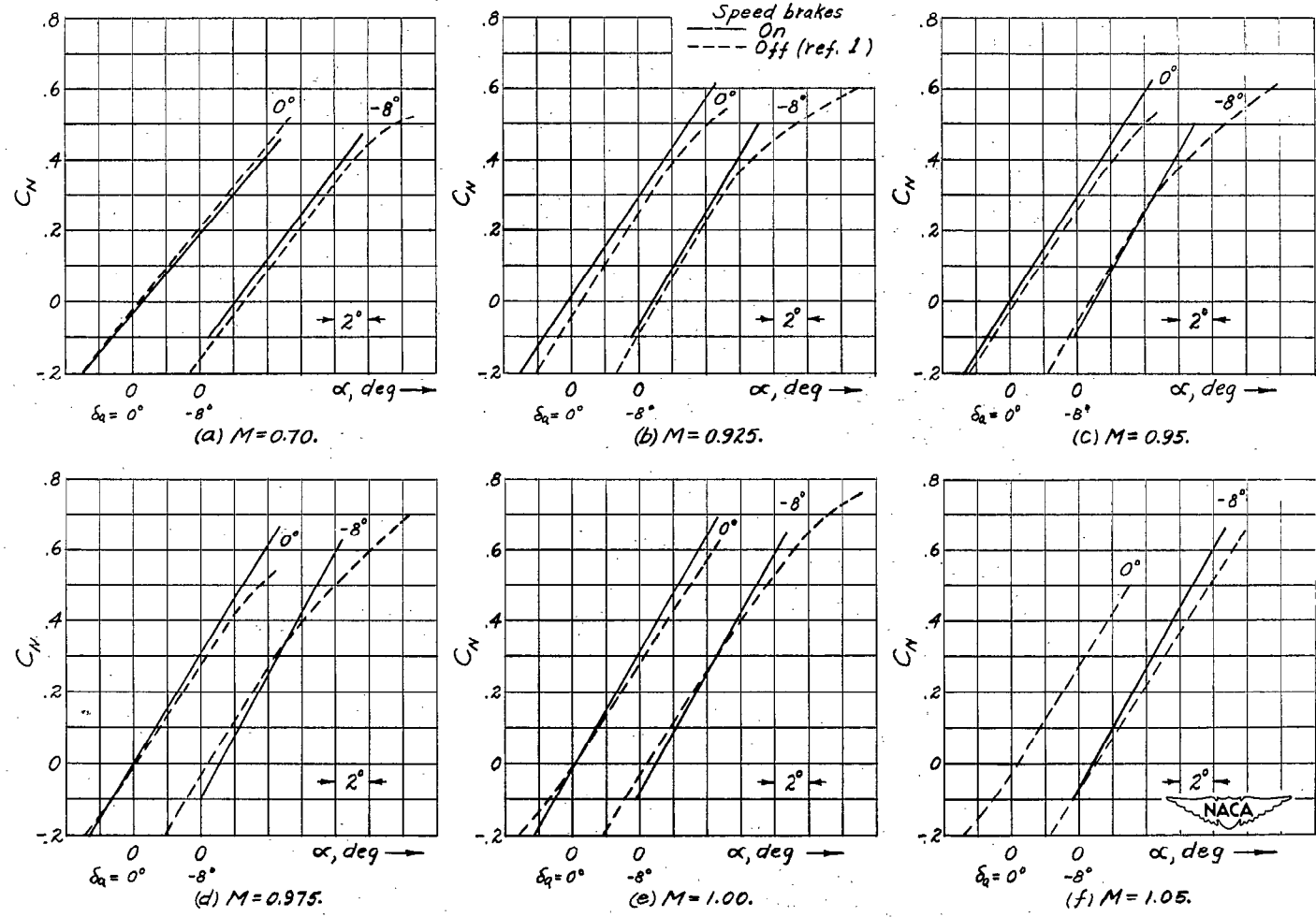
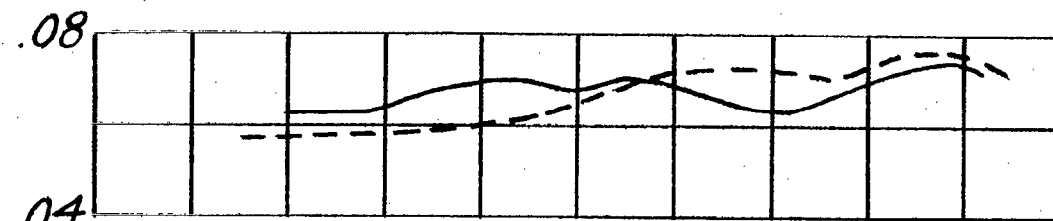


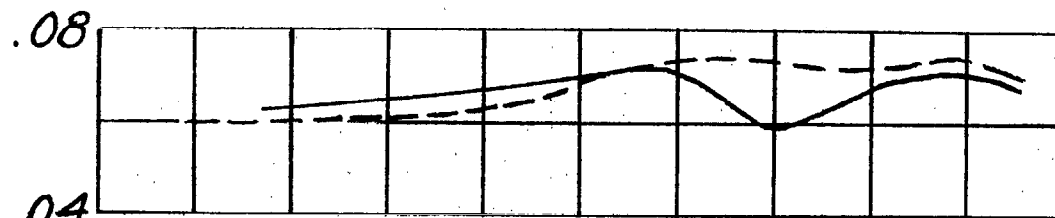
Figure 13.- Variation of normal-force coefficient with angle of attack at several Mach numbers for two ailerator deflections with speed brakes on. Results from reference 1 with speed brakes off shown for comparison.

————— *Fin off*
 - - - - - *Fin on (reference 1)*

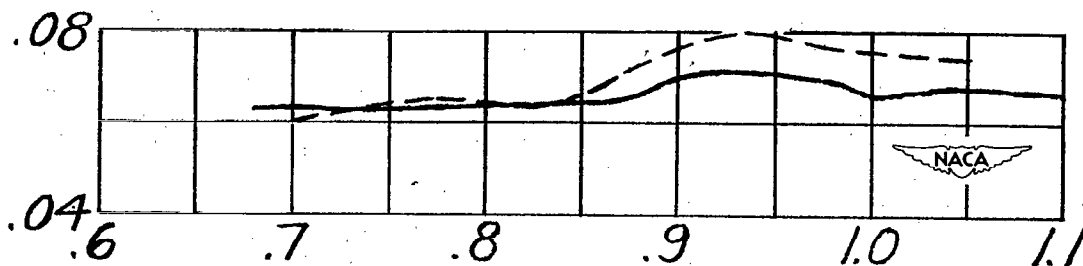


(a) $\delta_a = 0^\circ$.

$dC_N/d\alpha$



(b) $\delta_a = -4.9^\circ$.



(c) $\delta_a = -8^\circ$.

Figure 14.- Variation of normal-force-curve slope with Mach number for several ailerator deflections with fin off. Results from reference 1 with fin on shown for comparison.

Speed brakes

— On
 - - - Off (ref. 1)

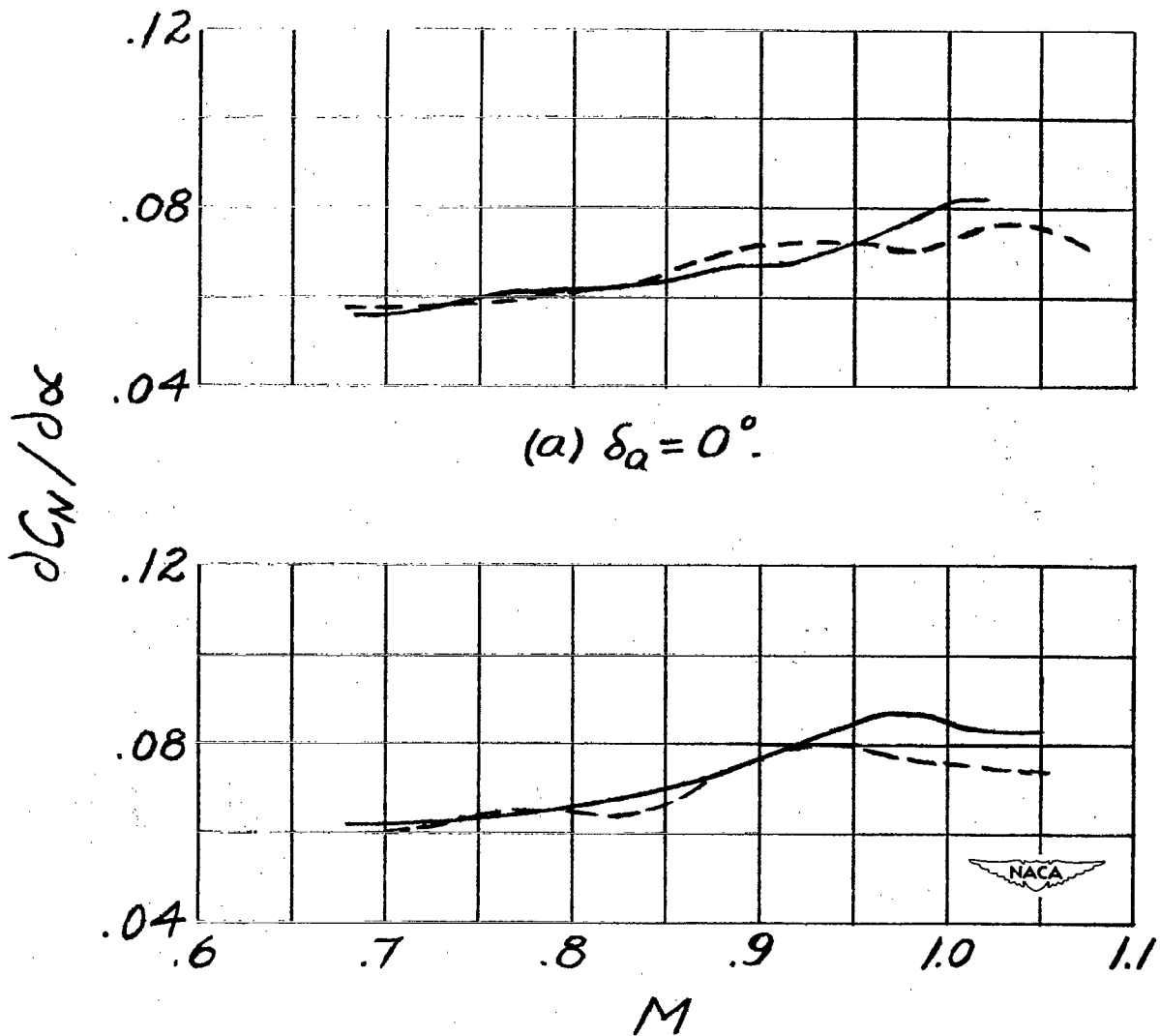
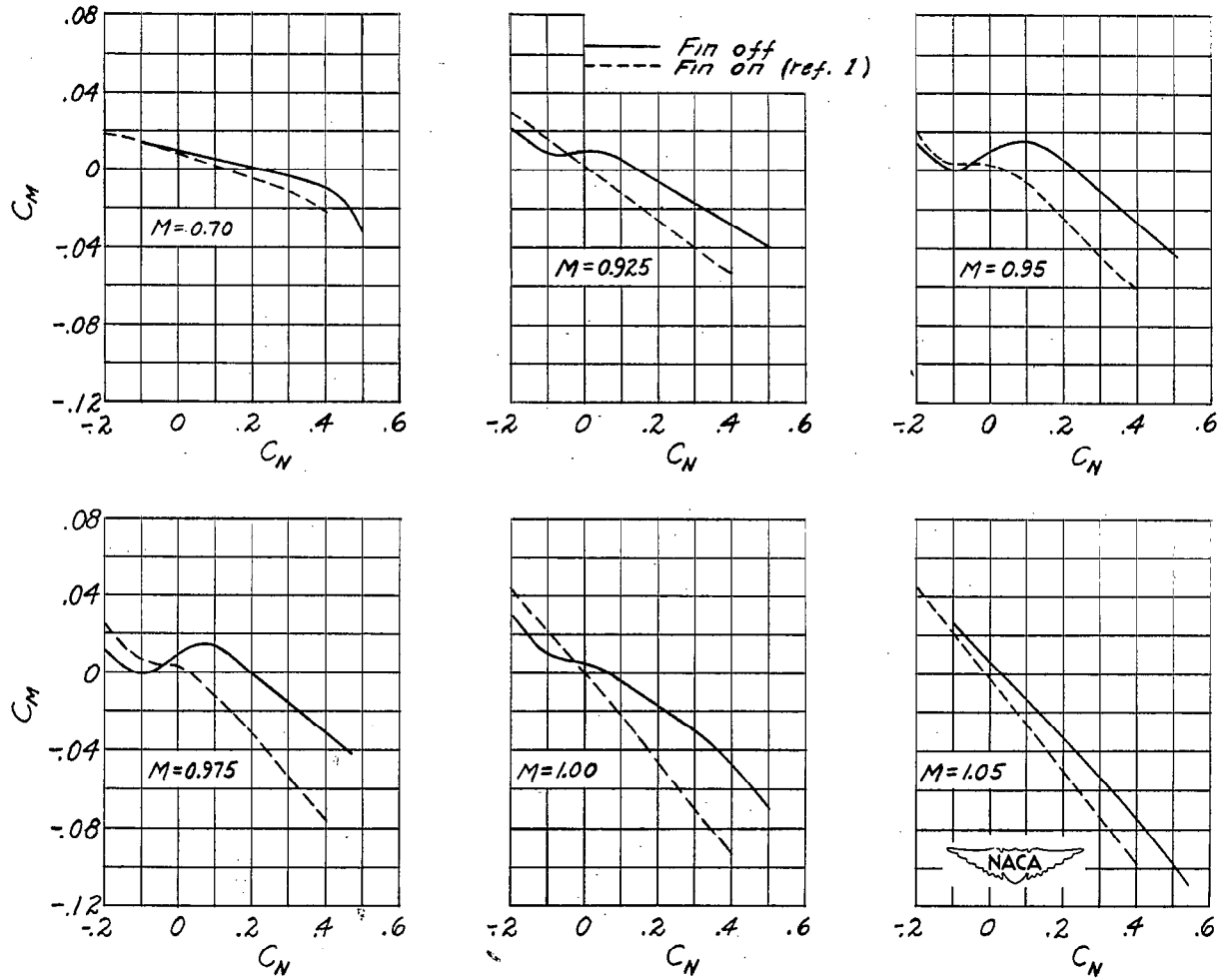
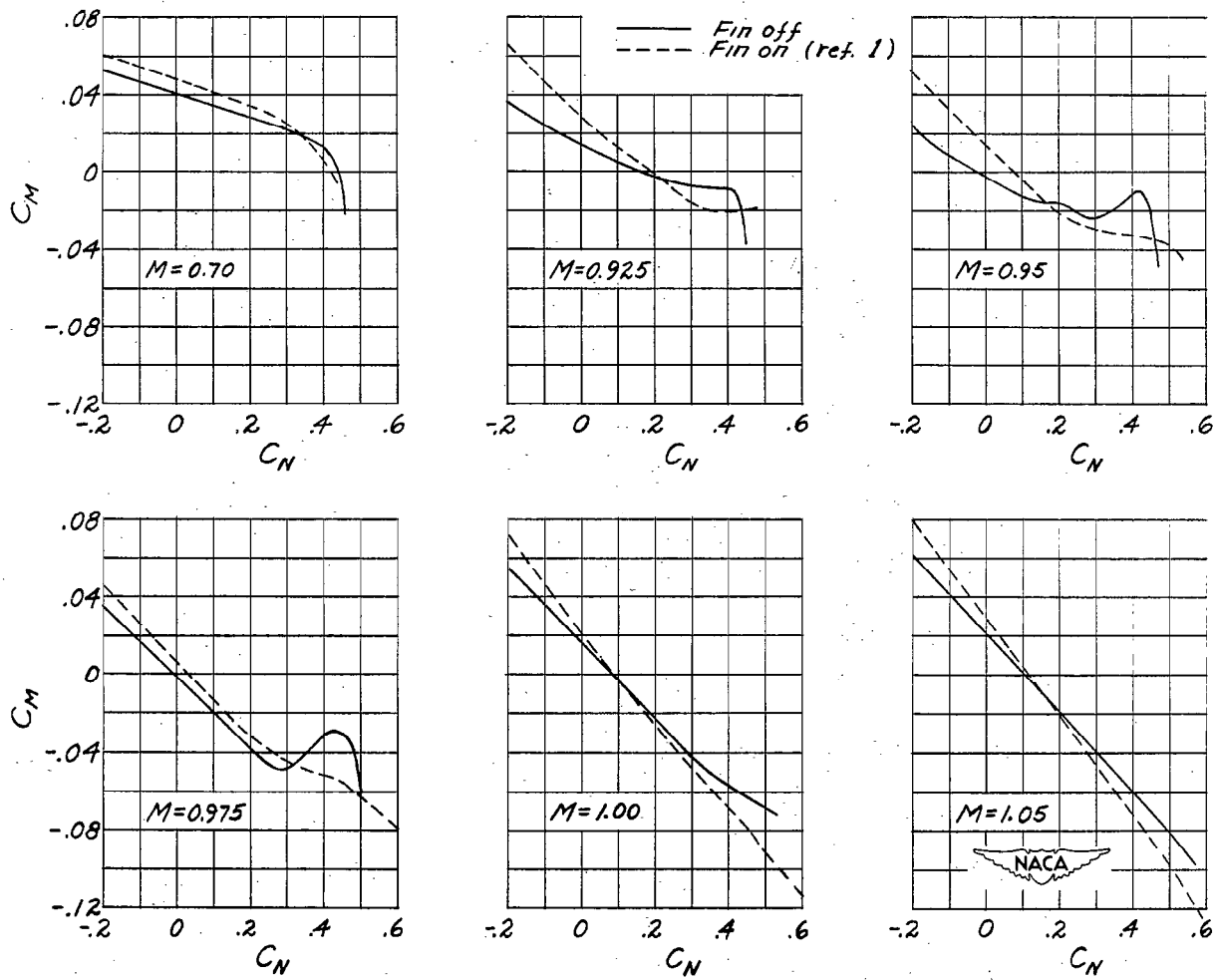


Figure 15.- Variation of normal-force-curve slope with Mach number at two ailerator deflections with speed brakes on. Results from reference 1 with speed brakes off shown for comparison.



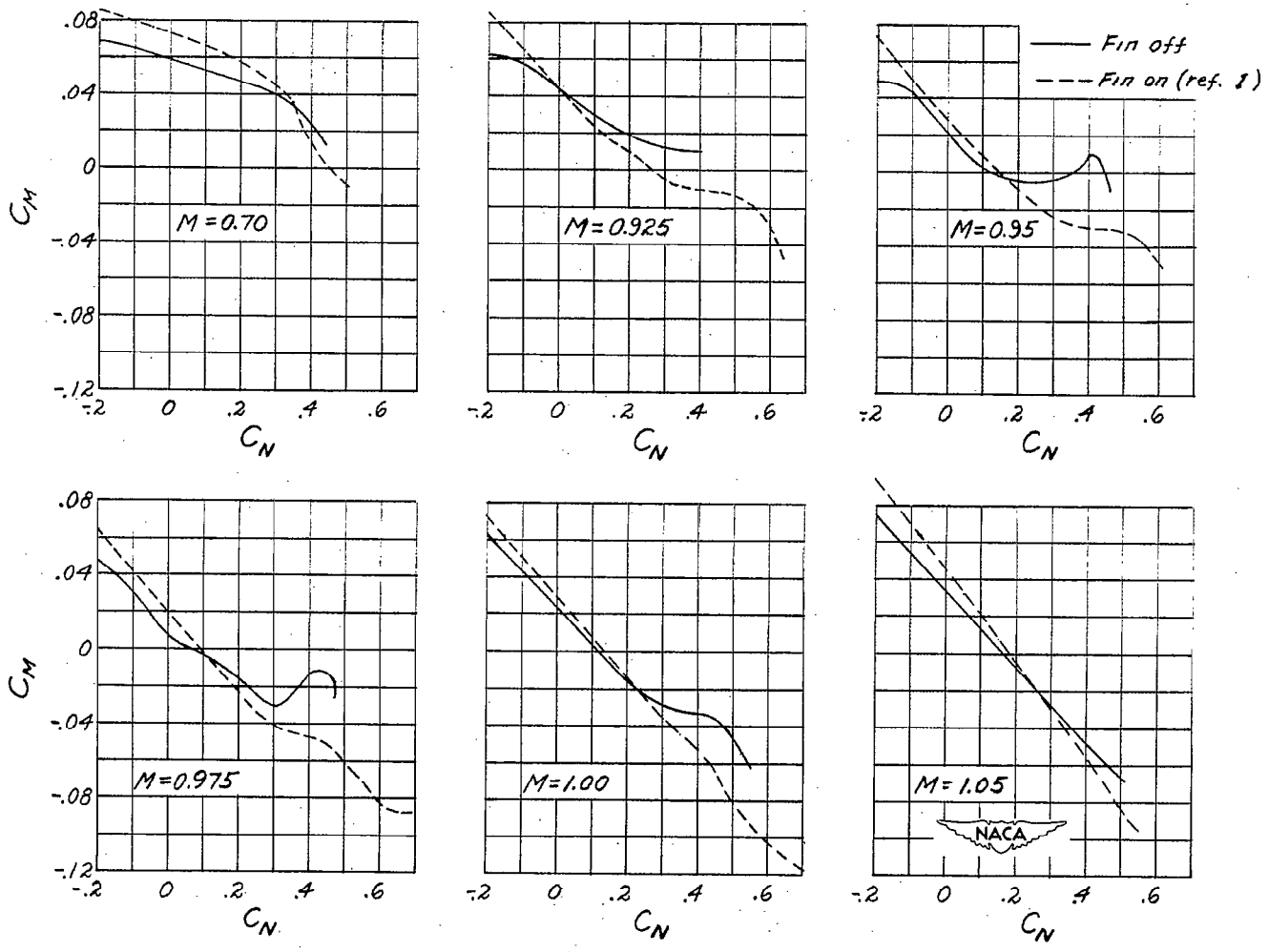
(a) $\delta_a = 0^\circ$.

Figure 16.- Variation of pitching-moment coefficient with normal-force coefficient at several Mach numbers for several ailerator deflections with fin off. Results from reference 1 with fin on shown for comparison.



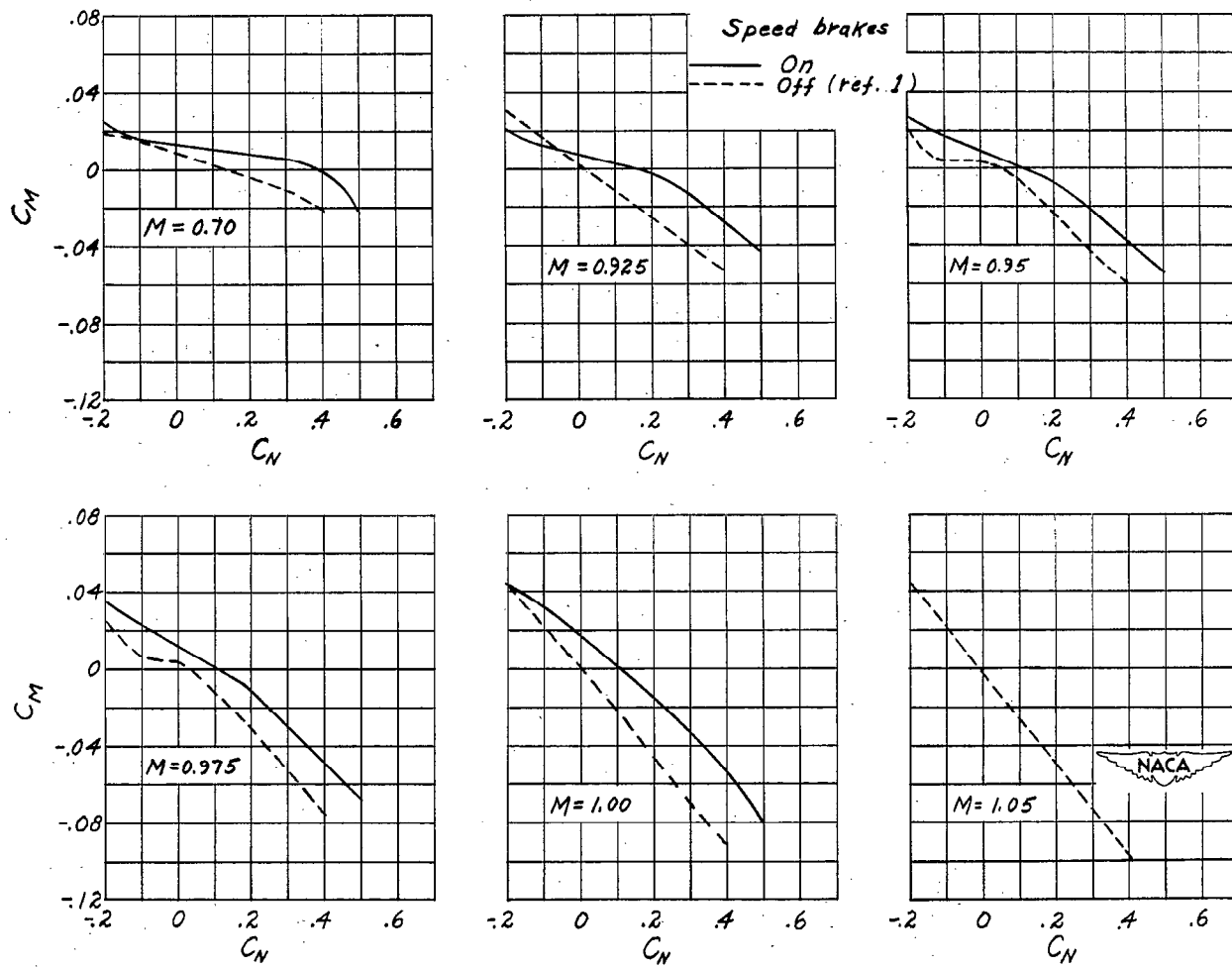
(b) $\delta_a = -4.9^\circ$.

Figure 16.- Continued.



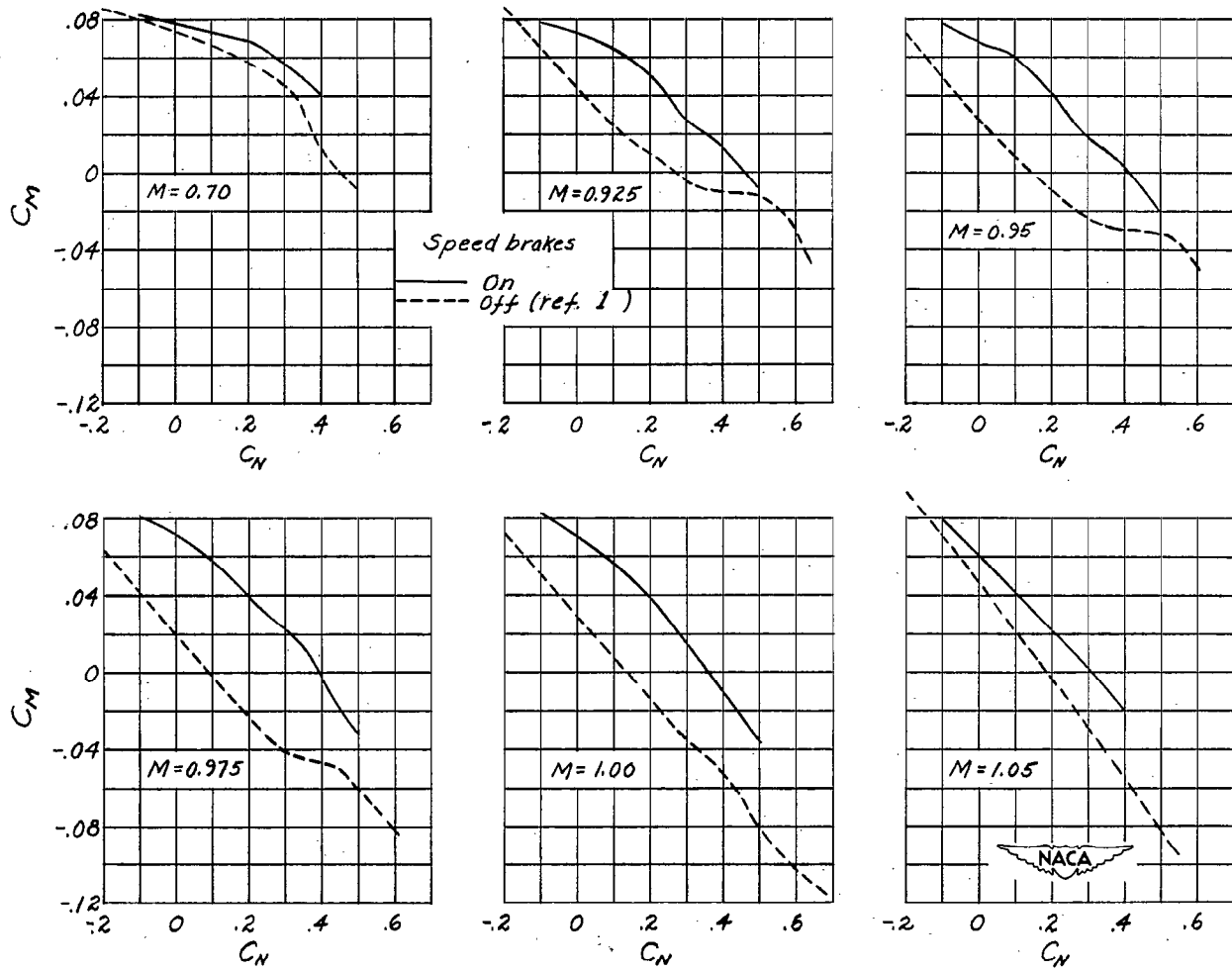
(c) $\delta_a = -8.0^\circ$.

Figure 16.- Concluded.



(a) $\delta_a = 0^\circ$.

Figure 17.- Variation of pitching-moment coefficient with normal-force coefficient at several Mach numbers for two ailerator deflections with speed brakes on. Results from reference 1 with speed brakes off shown for comparison.



(b) $\delta_a = -8.0^\circ$.

Figure 17.- Concluded.

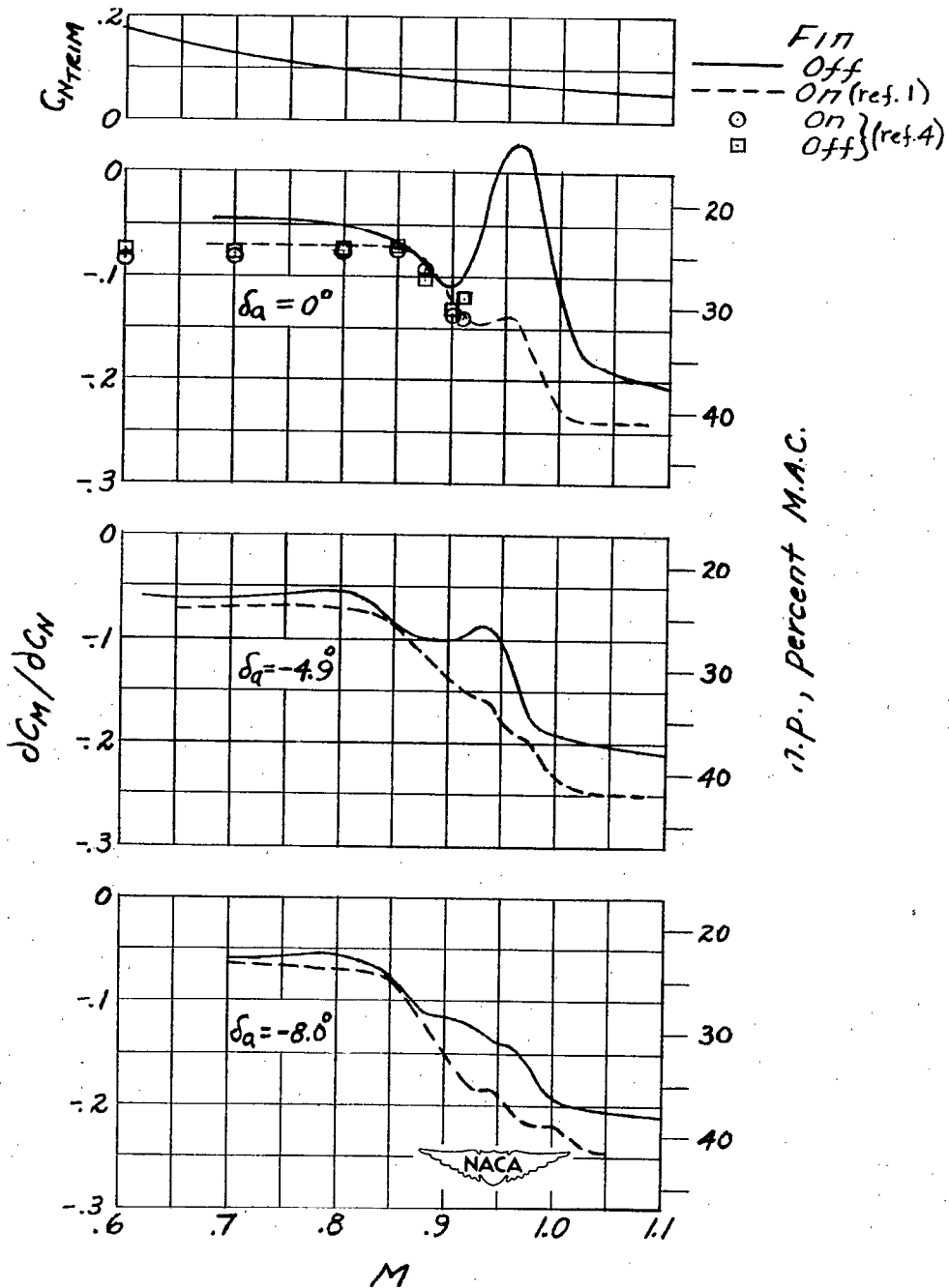


Figure 18.- Variation with Mach number of slope of pitching-moment curve $\frac{\partial C_M}{\partial C_N}$ for several ailerator deflections with fin off. Results from references 1 and 4 shown for comparison. Normal-force coefficient for level flight at 30,000 feet with wing loading of 28 also shown.

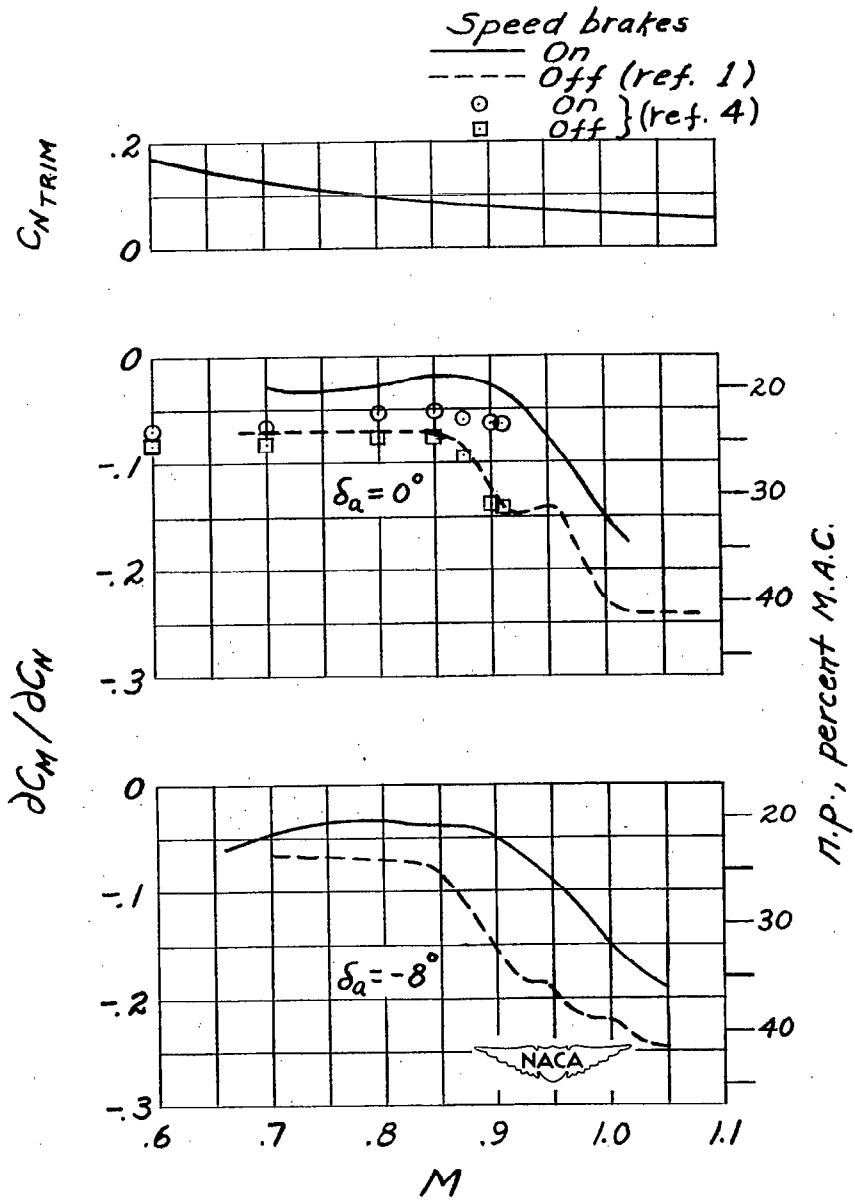
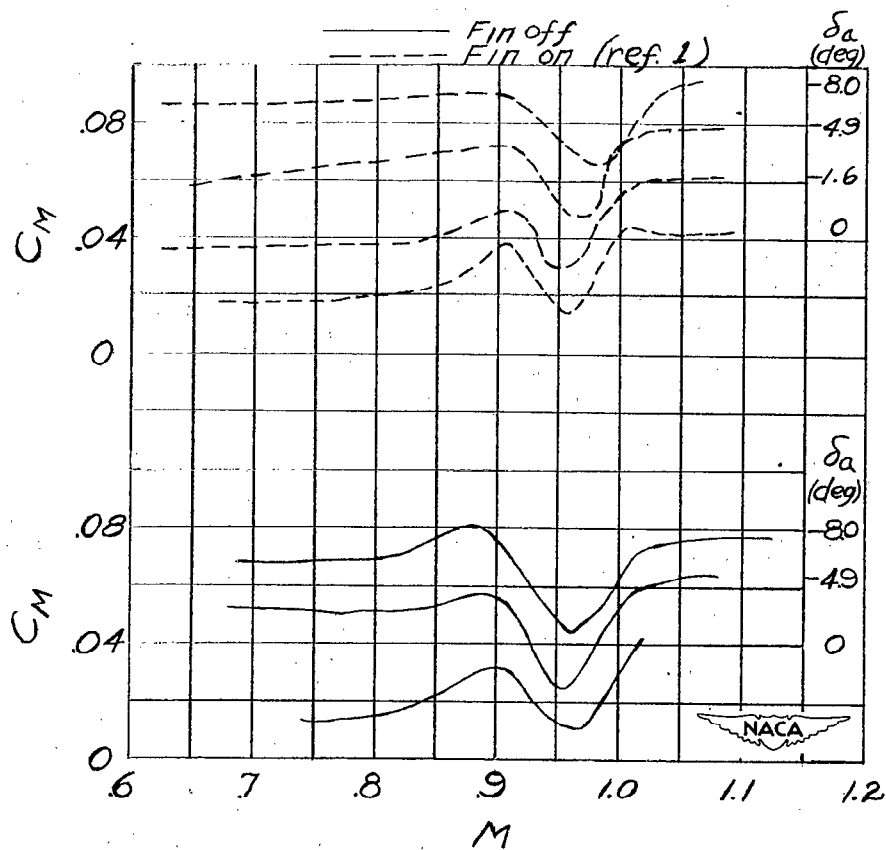
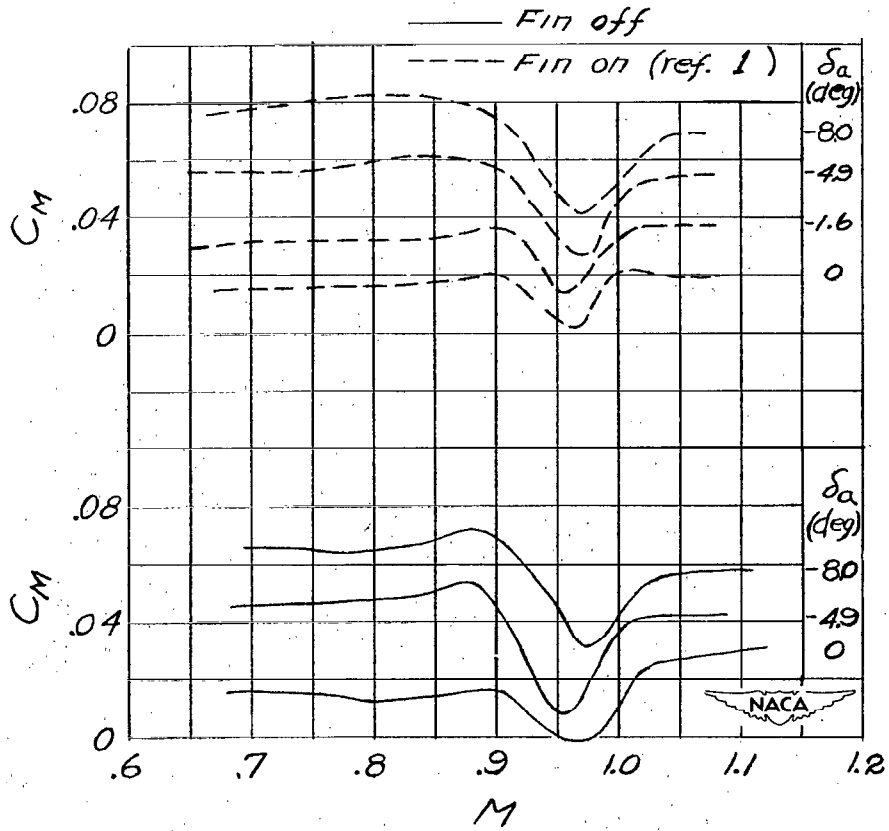


Figure 19.- Variation with Mach number of slope of pitching-moment curve $\frac{dC_M}{dC_N}$ for two ailerator deflections with speed brakes on. Results from references 1 and 4 shown for comparison. Normal-force coefficient for level flight at 30,000 feet with wing loading of 28 also shown.



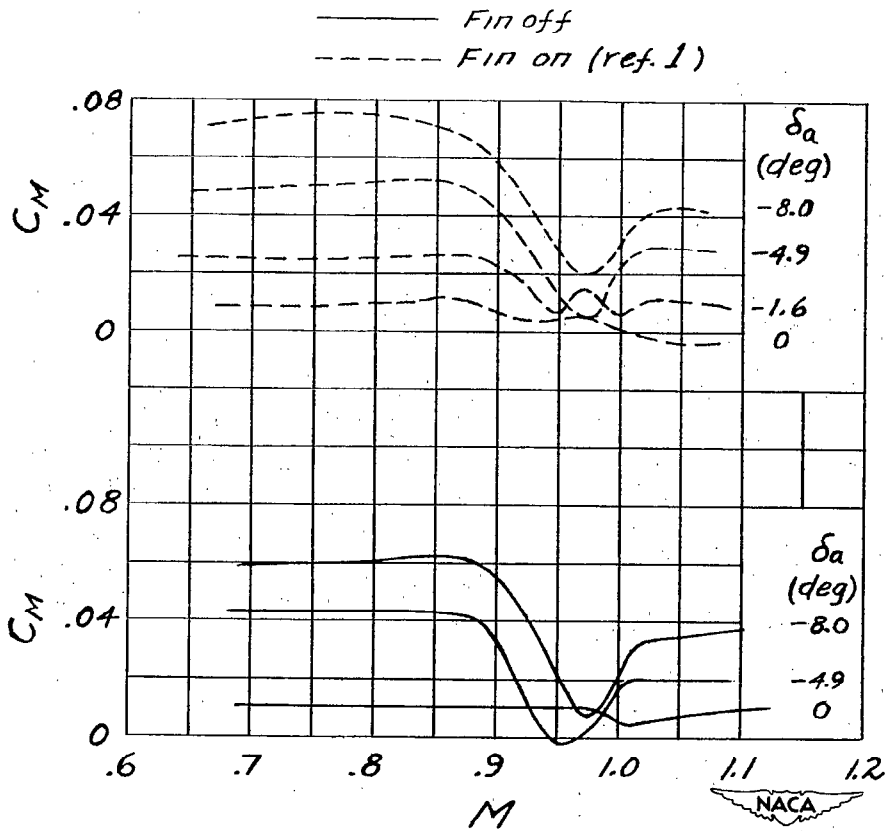
(a) C_N = -0.2.

Figure 20.- Variation of pitching-moment coefficient with Mach number at several ailerator deflections for several normal-force coefficients with fin off. Results from reference 1 with fin on shown for comparison.



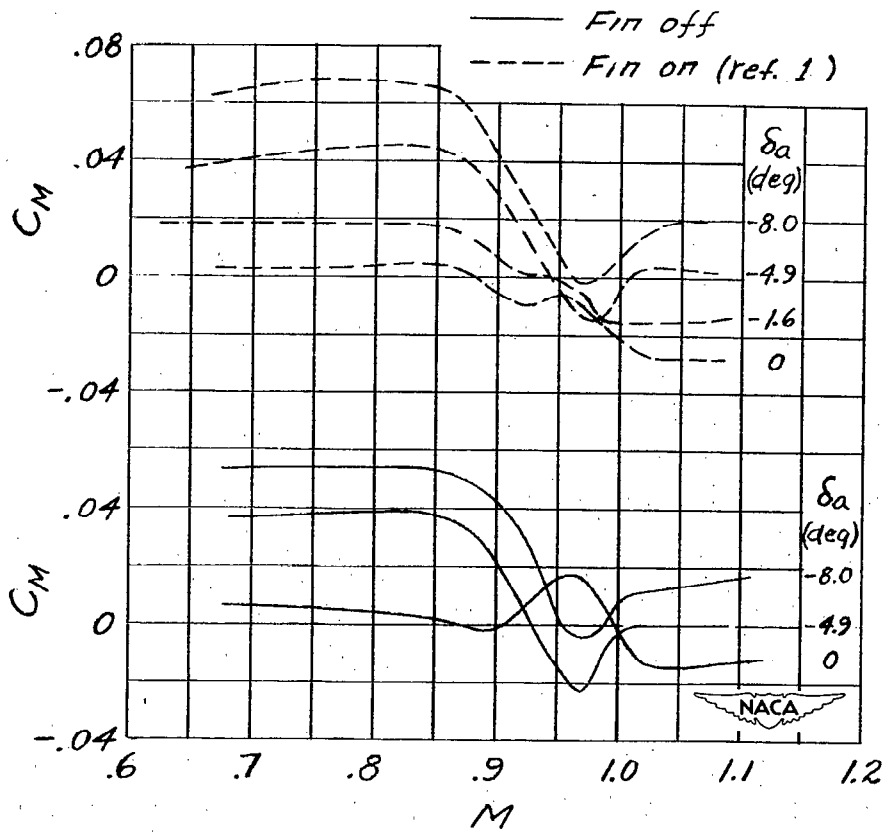
(b) $C_N = -0.1$.

Figure 20.- Continued.



(c) $C_N = 0$.

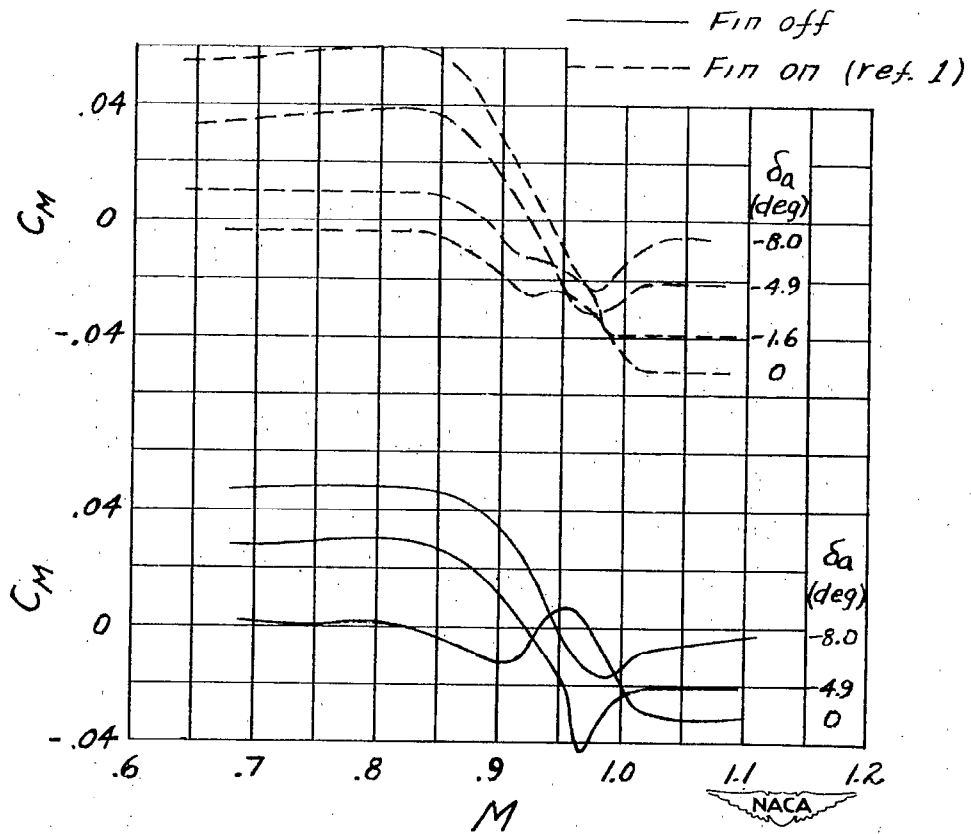
Figure 20.- Continued.



(d) $C_N = 0.1$.

Figure 20.- Continued.

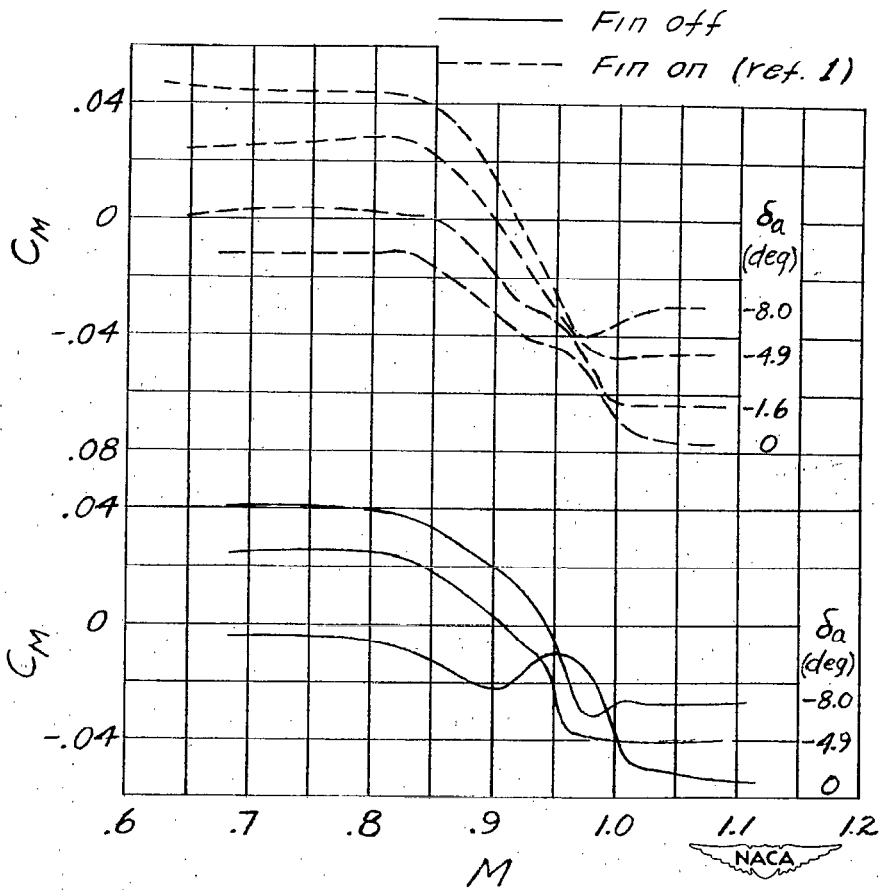
~~CONFIDENTIAL~~



(e) $C_N = 0.2$.

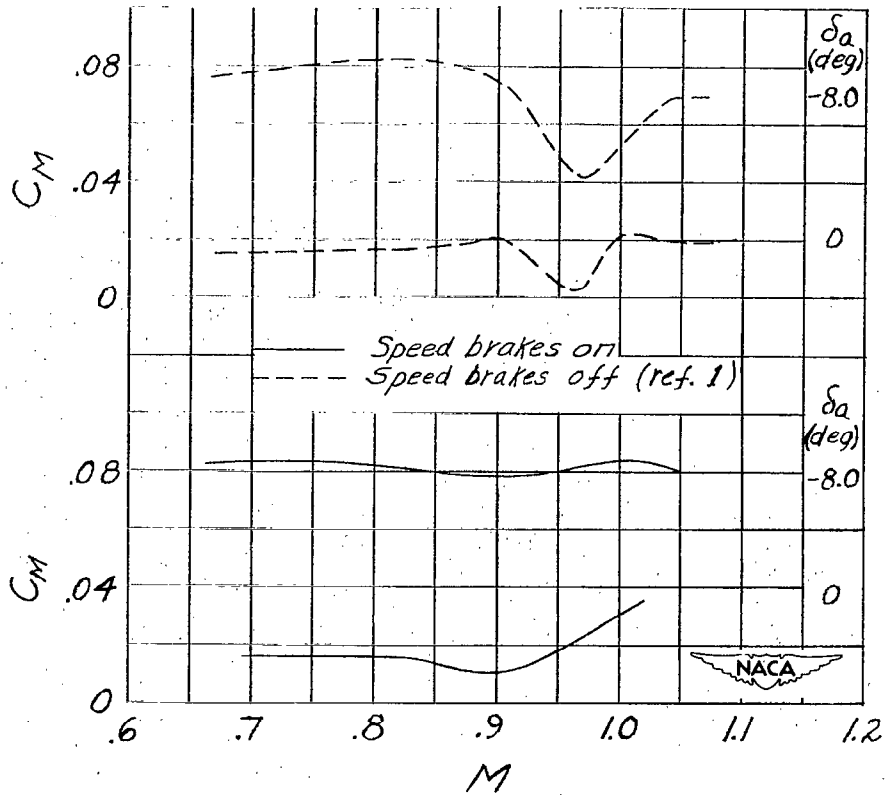
Figure 20.- Continued.

~~CONFIDENTIAL~~



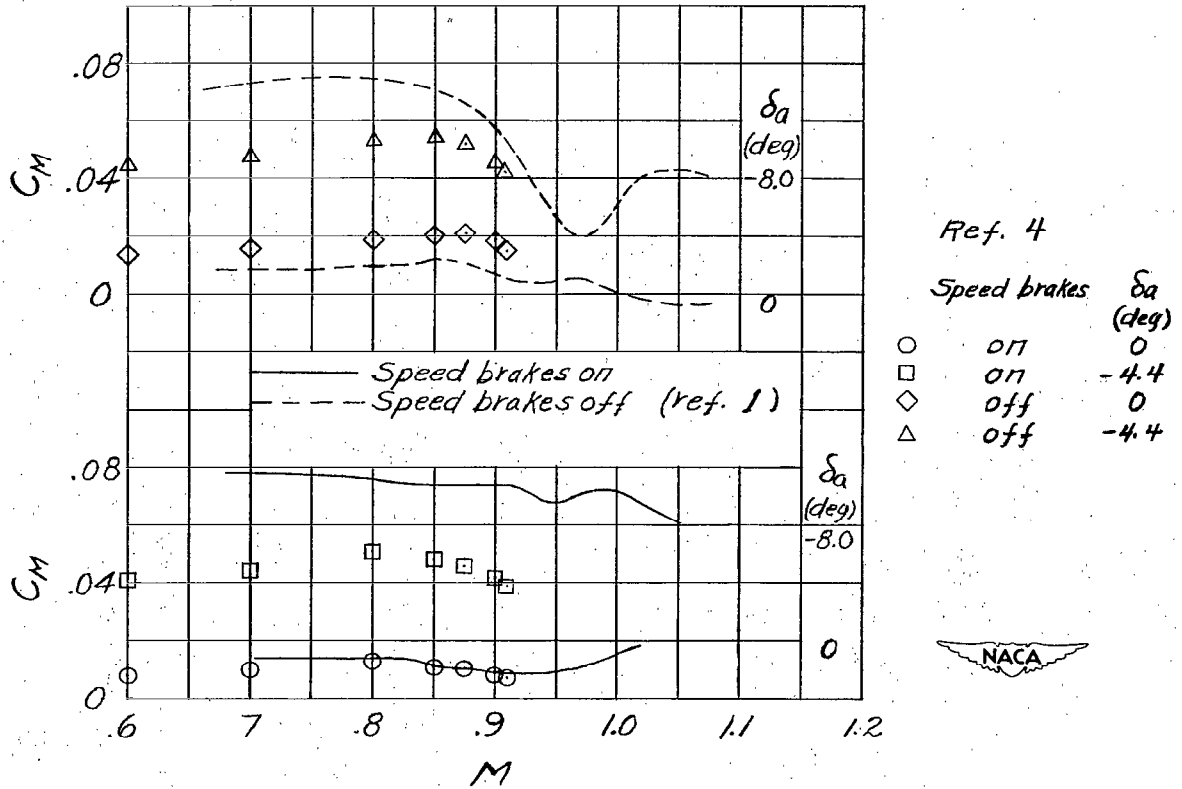
(f) $C_N = 0.3$.

Figure 20.- Concluded.



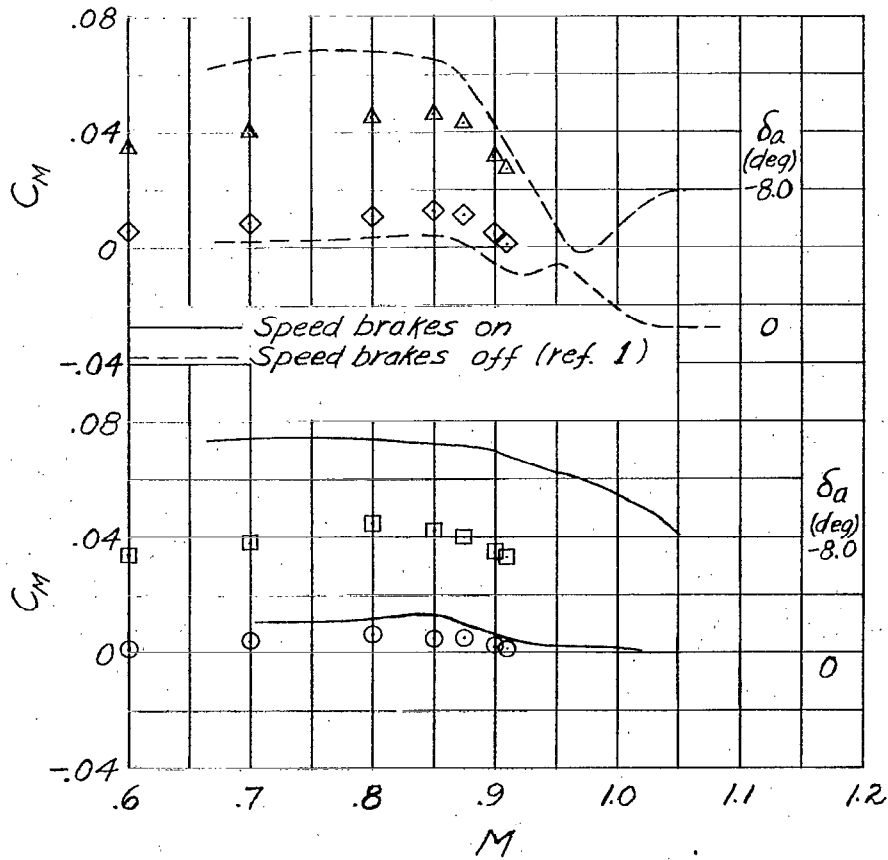
(a) $C_N = -0.1$.

Figure 21.- Variation of pitching-moment coefficient with Mach number at two ailerator deflections for several normal-force coefficients with speed brakes on. Results from reference 1 with speed brakes off shown for comparison.



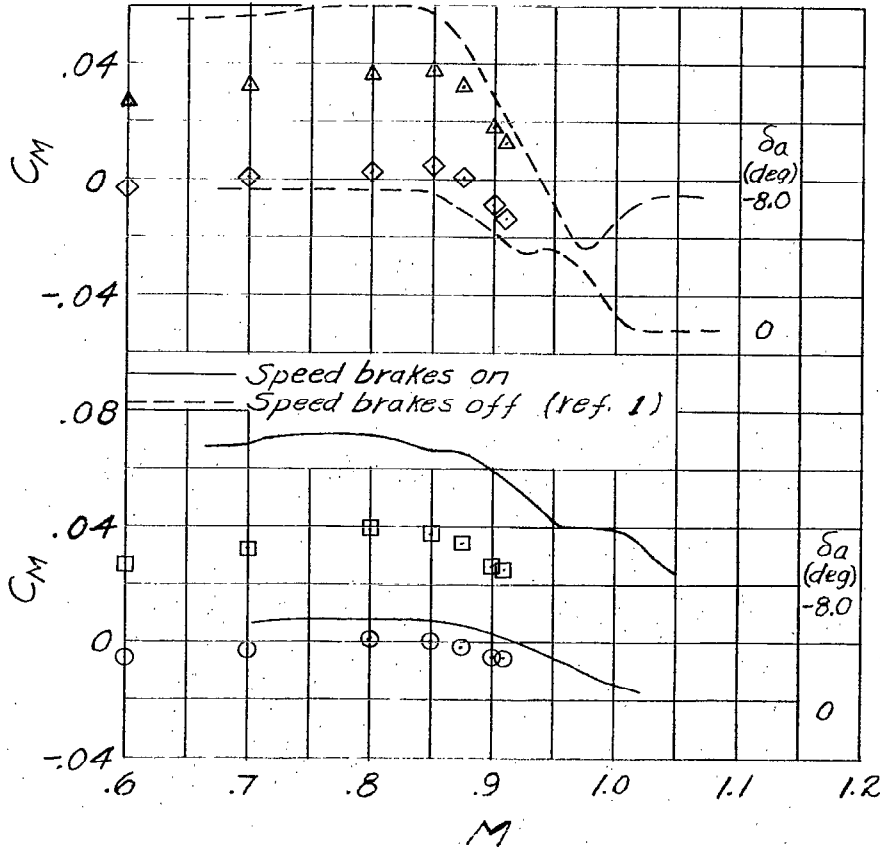
(b) $C_N = 0$.

Figure 21.- Continued.



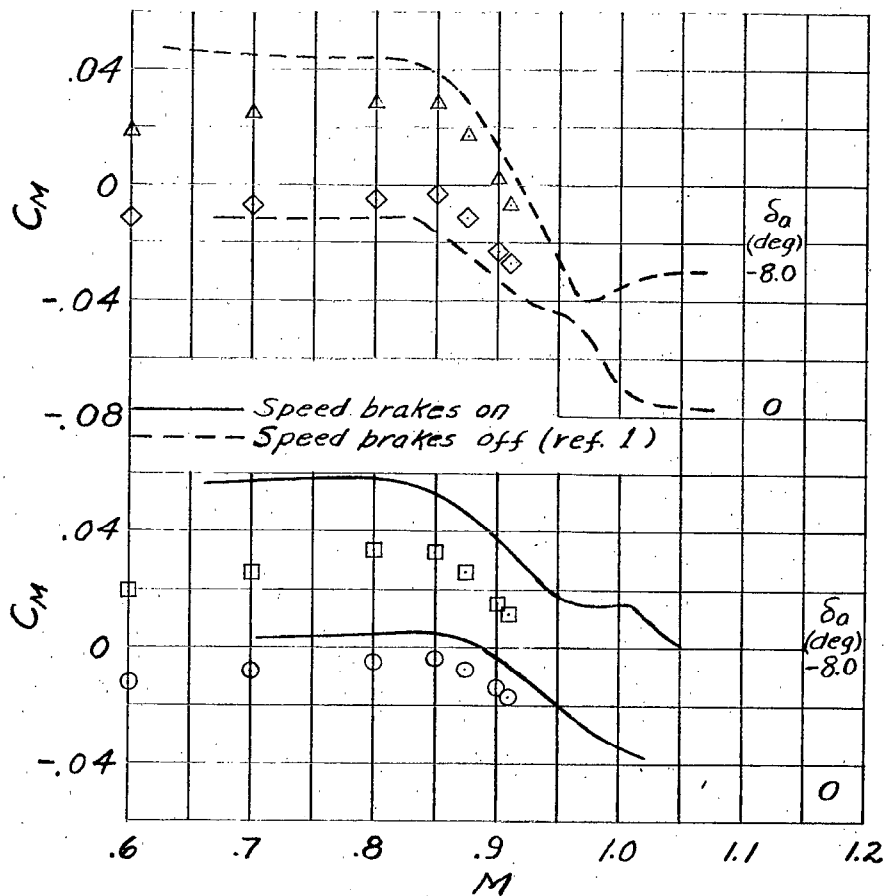
(c) C_N = 0.1.

Figure 21.- Continued.



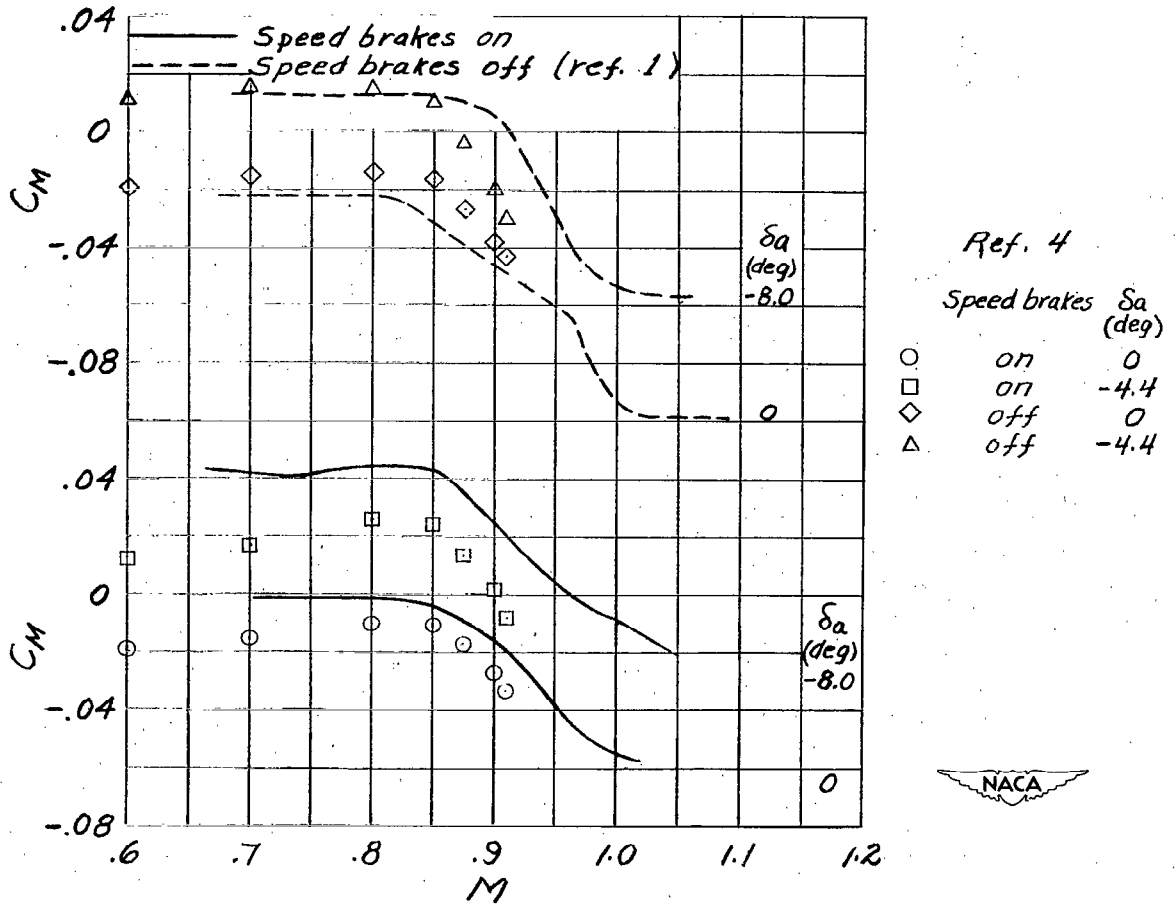
(d) $C_N = 0.2$.

Figure 21.- Continued.



(e) $C_N = 0.3$.

Figure 21.- Continued.



(f) $C_N = 0.4$.

Figure 21.- Concluded.

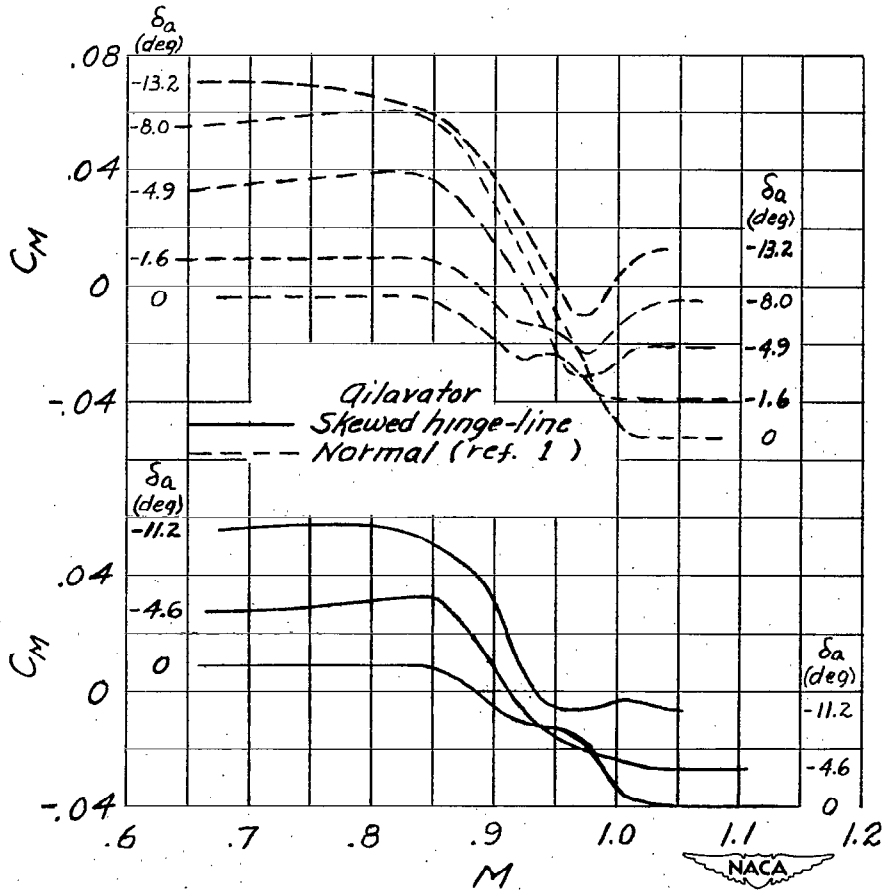


Figure 22.- Variation of pitching-moment coefficient with Mach number at several deflections of ailerator having highly sweptback hinge line at a normal-force coefficient of 0.2. Results from reference 1 with normal ailerators shown for comparison.



NASA Technical Library



3 1176 01438 5430

